

LONGITUDINAL FORCE CHARACTERISTICS OF SNOW TYRES USING COUPLED FEM-SPH METHOD

A THESIS

Submitted by

ARUNNELSON X

For the award of the degree

of

MASTER OF SCIENCE

(by Research)



**DEPARTMENT OF ENGINEERING DESIGN
INDIAN INSTITUTE OF TECHNOLOGY MADRAS
CHENNAI-600036**

AUGUST 2017

THESIS CERTIFICATE

This is to certify that the thesis entitled “**LONGITUDINAL FORCE CHARACTERISTICS OF SNOW TYRES USING COUPLED FEM-SPH METHOD**”, submitted by **Arunnelson X** to the Indian Institute of Technology Madras, for the award of the degree of **Master of Science (by Research)** is a bonafide record of research work carried out by him under my supervision. The contents of this thesis, in full or in parts, have not been submitted to any other Institute or University for the award of any degree or diploma.

Prof. R. Krishna Kumar

Research Guide

Professor

Dept. of Engineering Design

IIT-Madras, 600036

Place: Chennai

Date: 14-August-2017

ACKNOWLEDGEMENT

My research life at IIT Madras has been a wonderful journey for me. This wonderful journey cannot be completed, without thanking everyone who accompanied me in my journey. First of all, I express my heartfelt thanks and immense gratitude to my research guide Prof. R. Krishna Kumar, who helped me, guided me and continuously supported me throughout my research period. His enthusiasm and the expertise in several fields are always inspiring me. I am forever indebted to him for the opportunity he gave me. I thank Dr. K.V. Narasimha Rao, DGM, JK Tyres, to have shared his expertise in Finite Element modeling of tyres, and also for his technical and managerial support during the research period. I thank my General Test Committee for their valuable comments and suggestions. I thank all my lab mates and friends, with whom I often had conceptual discussions and the fun filled memorable time, we had. I thank Balu sir, for his perennial availability at times of need. Finally, I take this opportunity to thank my family members, who have always been by my side in all times. I have no words to thank them for the patience and the support offered by them.

Arunnelson X

ABSTRACT

KEY WORDS: *Snow, Tyre, Sipes, Finite Element, Smoothed Particle Hydrodynamics, Hydroplaning, Traction, Motion resistance*

Performance and handling of a wheeled vehicle in snow are different from an asphalt road, because of the complex mechanics between snow and the tread and the nonlinear behavior of snow and tyre. The interfacial forces at the contact area define the performance of a vehicle. The differences between winter tyres and summer tyres are sipes in the tread block and the tread material that has a low glass transition temperature. Most of the available literature used smooth cap tyre to simulate tyre-snow interaction, due to the restrictions in Finite Element Method (FEM). To overcome the restrictions of mesh, a meshfree method is needed.

The major aim of this work is to develop a methodology for snow tyres. In this work, Lagrangian FEM, Coupled Eulerian Lagrangian (CEL), Smoothed Particle Hydrodynamics (SPH) numerical methods have been compared to simulate tyre-snow interaction using plate-sinkage, tyre indentation and tread indentation tests. From these comparisons, SPH employed with cubic kernel function provided better results.

The frictional energy in contact area melts the snow and creates a thin water layer between tyre and snow which reduces the solid to solid contact. Sipes play a significant role by digging the water in the contact area and re-establishes solid to solid contact between tyre and snow. This makes the prediction of interfacial forces at the contact area a challenge and is incomplete without considering the effects of sipes. The difference in coefficient of friction has been calculated from numerical simulation of single tread block with water for both the cases, viz. with and without sipes using coupled FEM-SPH method. Tyre with sipes showed a higher critical velocity in hydroplaning when compared to smooth cap tyre and block patterned tread tyre.

A numerical procedure for the interaction of the pneumatic tyre and snow by coupling Lagrangian FEM and SPH with the inclusion of the effect of sipes using an equivalent friction coefficient. An elasto-plastic model (modified Drucker-Prager Cap model) is used to model snow and the material properties are chosen from the literature. The variation of traction and motion resistance with respect to torque is obtained for

various cases such as smooth cap tyre, block patterned tread tyre with and without sipes for soft and hard snow, and also for various loads. In this study, SIMULIA/Abaqus has been used to perform all numerical simulations.

TABLE OF CONTENTS

ACKNOWLEDGEMENTS	i
ABSTRACT	ii
LIST OF TABLES	vii
LIST OF FIGURES	viii
ABBREVIATIONS	xii
NOTATION	xiii
1 INTRODUCTION	1
1.1 Introduction.....	1
1.2 Research Background	2
1.3 Motivation.....	4
1.4 Smoothed Particle Hydrodynamics (SPH).....	5
1.4.1 Kernel Approximation	5
1.4.2 Particle Approximation.....	6
1.4.3 Total Lagrangian Formulation for SPH	7
1.5 Modified Drucker-Prager Cap Model.....	11
1.6 Sponge Effect.....	14
1.7 Objective and Scope of the Research.....	16
1.8 Organisation of the Thesis	17
2 THE MECHANISM OF TYRE TRACTION IN SNOW	18
2.1 Forces Act on Tyre.....	18
2.1.1 Motion Resistance Force.....	19

2.1.2 Force due to Compressed Snow in Grooves	19
2.1.3 Traction Force	19
2.1.4 Rolling Resistance Force	19
2.2 Summary	20
3 COMPARISON OF FEM, CEL AND SPH NUMERICAL METHODS	22
3.1 Introduction.....	22
3.2 Plate-Sinkage Test	22
3.3 Tyre Indentation Test	25
3.4 Tread Indentation Test	27
3.5 Summary	28
4 IMPORTANCE OF SIPES	29
4.1 Introduction.....	29
4.2 Tyre Hydroplaning Simulations.....	29
4.3 Friction Coefficient Difference Between Blocks With and Without Sipes .	32
4.4 Summary	33
5 LONGITUDINAL SLIP-FORCE CHARACTERISTICS	35
5.1 Particle Density Study.....	35
5.2 Simulation Procedure to Obtain Longitudinal slip-Force Curve for Snow Tyres	36
5.2.1 Tyre Axis System.....	36
5.2.2 Finite Element Model of a Pneumatic Tyre	36
5.2.3 Procedure to Obtain Longitudinal slip-Force Characteristics.....	38
5.3 Is Longitudinal slip-Force Curve Suitable for Snow Tyres?	40
5.4 Summary.....	43

6 TORQUE-FORCE CHARACTERISTICS	44
6.1 Finite Element Modeling and Procedure	44
6.2 Force Characteristics of Smooth, Block Patterned and Block Patterned Tread with Sipes Tyres in Soft Snow	45
6.3 Force Characteristics of Smooth, Block Patterned and Block Patterned Tread with Sipes Tyres in Hard Snow	49
6.4 Comparison of Tyre Performance in Soft and Hard Snow	51
6.5 Comparison of Tyre Performance with Different Loads	53
6.6 Computational Time	55
6.6.1 Comparison of the Computational Time of Lagrangian, CEL and SPH Methods.....	55
6.6.2 Computational Time to Obtain Torque-Force Characteristics.....	56
 7 CONCLUSION	 57
7.1 Conclusions.....	57
7.2 Scope of Future Work.....	58
 APPENDIX	 59
 REFERENCE	 61

LIST OF TABLES

Table 3.1: Parameters for Modified Drucker-Prager Cap model.....	23
Table 3.2: Hardening law.....	24
Table 3.3: Plate-Sinkage comparison with vertical displacement of plate into snow .	24
Table 3.4: Contact area of loaded rib tyre in different numerical snow model	27
Table 4.1: Equation of state parameter for water in linear $U_s - U_p$ Hugoniot form	29
Table 4.2: Critical velocity of hydroplaning.....	32
Table 4.3: Variation of Longitudinal force and Friction coefficient with load	33
Table 5.1: Plate-Sinkage test comparison with different distance between particles .	36
Table 5.2: Elastic properties of different reinforcement.....	37
Table 5.3: REBAR parameter for different reinforcements.....	37
Table 5.4: Reduced polynomial model parameter for different rubber region	38
Table 6.1: Computational time comparison of Lagrangian, CEL and SPH methods ..	55

LIST OF FIGURES

Figure 1.1: Kelirengas tyre	1
Figure 1.2: Block patterned tread tyre with sipes	2
Figure 1.3: A schematic of Literature review	4
Figure 1.4: A schematic of implementation of SPH in Total Lagrangian formulation	10
Figure 1.5: The yield surface of Modified Drucker-Prager Cap model in meridional plane.....	11
Figure 1.6: The pressure-plastic volumetric strain relationship.....	12
Figure 1.7: The yield surface of Modified Drucker-Prager Cap model in deviatoric plane.....	13
Figure 1.8: The plastic flow potential in meridional plane.....	14
Figure 1.9: Natural snow behavior under vehicle load.....	15
Figure 1.10: Cut section of a loaded tyre on (a) Lagrangian (b) CEL with EVF contour and on (c) SPH snow blocks	15
Figure 2.1: Cut section of tyre-snow interaction shows forces act on the tyre.....	18
Figure 2.2: Deformed shape of the rolling tyre on snow (left) and on road (right) with the undeformed shape shown in red outline	20
Figure 3.1: Cut section of plate-sinkage analysis using (a) Lagrangian (b) CEL and (c) SPH with cubic kernel function with vertical displacement contours	25

Figure 3.2: Contact pressure (N/m ²) of a loaded rib tyre on (a) Lagrangian (b) CEL and on (c) SPH snow box.....	26
Figure 3.3: (a) Tread-snow assembly and Rut formed by the tread geometry in (b) Lagrangian (c) CEL and on (d) SPH snow blocks.....	27
Figure 4.1: Different Tread Geometry of (a) Smooth cap tyre (b) Block patterned tread tyre and (c) Block patterned tread tyre with Sipes.....	30
Figure 4.2: Tyre-water assembly for hydroplaning	31
Figure 4.3: Contact pressure of loaded (a) Smooth cap tyre, (b) Block patterned tread tyre and (c) Block patterned tyre with sipes	31
Figure 4.4: Contact area of rubber block with sipes (left) and without sipes (right) on rigid surface with water; Blue regions indicate water	32
Figure 5.1: Density contours for the cut sections of Plate-Sinkage tests with uniform node density of (a) 0.01 m, (b) 0.02 m and (c) 0.03 m	35
Figure 5.2: Local wheel coordinate as given in ISO 8855.....	36
Figure 5.3: FE model of tyre. (a) Inflated two-dimensional (2D) axisymmetric tyre model without tread (b) Adding a tread section to the three-dimensional (3D) tyre section model (c) Full 3D tyre model	37
Figure 5.4: Procedure to obtain longitudinal slip-force curve. (a) Loading and rolling the tyre on road (b) Rolling the tyre in snow to find zero slip condition (c) Series of analyses to find forces in each slip ratio	39
Figure 5.5: Variation of vertical position of rim node on road	40

Figure 5.6: Variation of tyre sinking depth and tyre contact area in snow	41
Figure 5.7: Variation of Traction, Motion Resistance and Drawbar pull	42
Figure 5.8: Frictional mechanism of a block over a surface.....	42
Figure 5.9: variation of Traction, Motion resistance and Drawbar pull with respect to torque for a smooth cap tyre	43
Figure 6.1: Procedure to obtain torque-force characteristics. (a) Inflated two-dimensional (2D) axisymmetric tyre model without tread (b) Adding a tread section to the three-dimensional (3D) tyre section model (c) Full 3D tyre model (d) Series of analyses to find forces under different torque.....	44
Figure 6.2: Rotational displacement of rim node.....	45
Figure 6.3: Variation of tyre sinking depth in soft snow	46
Figure 6.4: Variation of traction force in soft snow.....	47
Figure 6.5: Variation of net longitudinal force due to contact pressure in soft snow ..	48
Figure 6.6: Variation of drawbar pull in soft snow	48
Figure 6.7: Variation of drawbar pull in hard snow.....	49
Figure 6.8: Variation of traction force in hard snow	50
Figure 6.9: Variation of net longitudinal force due to contact pressure in hard snow .	50
Figure 6.10: Variation of tyre sinking depth in hard snow	51
Figure 6.11: Failure of compressed hard snow (left) and soft snow (right) in tread grooves with 200 Nm torque.....	52

Figure 6.12: Failure of compressed hard snow (left) and soft snow (right) in tread grooves with 600 Nm torque.....	52
Figure 6.13: Variation of vertical position of rim node with different loads.....	53
Figure 6.14: Variation of traction force with different loads.....	54
Figure 6.15: Variation of net longitudinal force due to contact pressure with different loads	54
Figure 6.16: Variation of drawbar pull with different loads	55
Figure A.1: Input file contains nodes and elements information.....	59
Figure A.2: SPH element creation	59
Figure A.3: Input parameters for SPH elements	60

ABBREVIATIONS

FEM	Finite Element Method
CEL	Coupled Eulerian Lagrangian
MPM	Material Point Method
SPH	Smoothed Particle Hydrodynamics
MPDC	Modified Drucker-Prager Cap
EVF	Element Volume Fraction
MRF	Motion Resistance Force
RRM	Rolling Resistance Moment
RRF	Rolling Resistance Force
Eos	Equation of state
3D	Three Dimensional
2D	Two Dimensional
RM2	Reaction Moment 2
MPE	Material Point Element

NOTATION

A	Function of a position vector
x (or) X	A three dimensional position vector
δ	Dirac delta function
Ω	Volume
h	Smoothing length
W	Kernel approximation function
N	Number particles within the smoothing length
m_j	Mass of particles j
ρ_j	Density of particles j
Δt	Time step
u	Displacement of material point
v	Velocity
a	Acceleration
σ	Cauchy stress tensor
P	Pioal-Krichhoff stress tensor
F	Deformation gradient
V_J^0	Initial volume of particle J
J	Jacobian, Determinant of deformation gradient tensor

E	Green strain tensor
$\dot{\varepsilon}$	Rate of deformation tensor
L	Velocity gradient
C	Material tangent modulus
c	Speed of sound
$\langle \rangle$	Smoothing approximation due to kernel function

CHAPTER 1

INTRODUCTION

1.1 INTRODUCTION

Transmission of forces in tyre depends on tyre construction, tread design, tread compound and the nature of terrain. Snow undergoes a large deformation from the applied force with properties changing rapidly with time, load, temperature and pressure. This phenomenon is called metamorphism (Colbeck 1982). This flexibility and metamorphism of snow makes handling and maneuverability of a vehicle more arduous and dangerous than asphalt road.

The idea of first pneumatic tyre was conceived by a Scottish engineer Robert William Thomson (Thomson 1847). However, his idea was not commercialized. The practical pneumatic tyre was discovered by John Boyd Dunlop (Dunlop 1890) as an upgrade to the bicycle. After four decades of tyre discovery, Nokian tyres introduced the first commercial winter tyre in 1934 by the name of Kelirengas (shown in Figure 1.1), was developed for Lorries, and also two years later, the first commercial passenger car winter tyre, Hakkapeliitta was introduced (Nokian Winter tyres Broucher, 2016).



Figure 1.1: Kelirengas tyre

(Source: <https://www.nokiantyres.com/company/about-us/history/over-80-years-since-the-invention-of-the-winter-tyre/first-winter-tyres/>)

Later, chains and studs have been introduced in winter tyre to increase the biting action in ice and snow. However, the chains and studs damaged the pavement and

generated unhealthy PM10 (particle with diameter less than 10 μm) powdered road-dust (Fukuzaki, Yanaka, and Urushiyama 1986), which made countries like Japan to forbid the usage of studded tyres from April 1, 1991 (Fukuoka 1994). European regulations for winter equipment on trucks and buses (Continental Truck Tyre Report, 2016) showed that, many of the European countries have banned and put restrictions on the use of studded and chained tyres. This motivated researchers to develop studless winter tyre with higher frictional characteristics to improve tyre performance without studs and chains. To achieve this, sipes have been added to the tyres. Sipes are small slits made in the tread to create teeth like projections as shown in Figure 1.2. The importance of sipes is discussed later in Chapter 4.

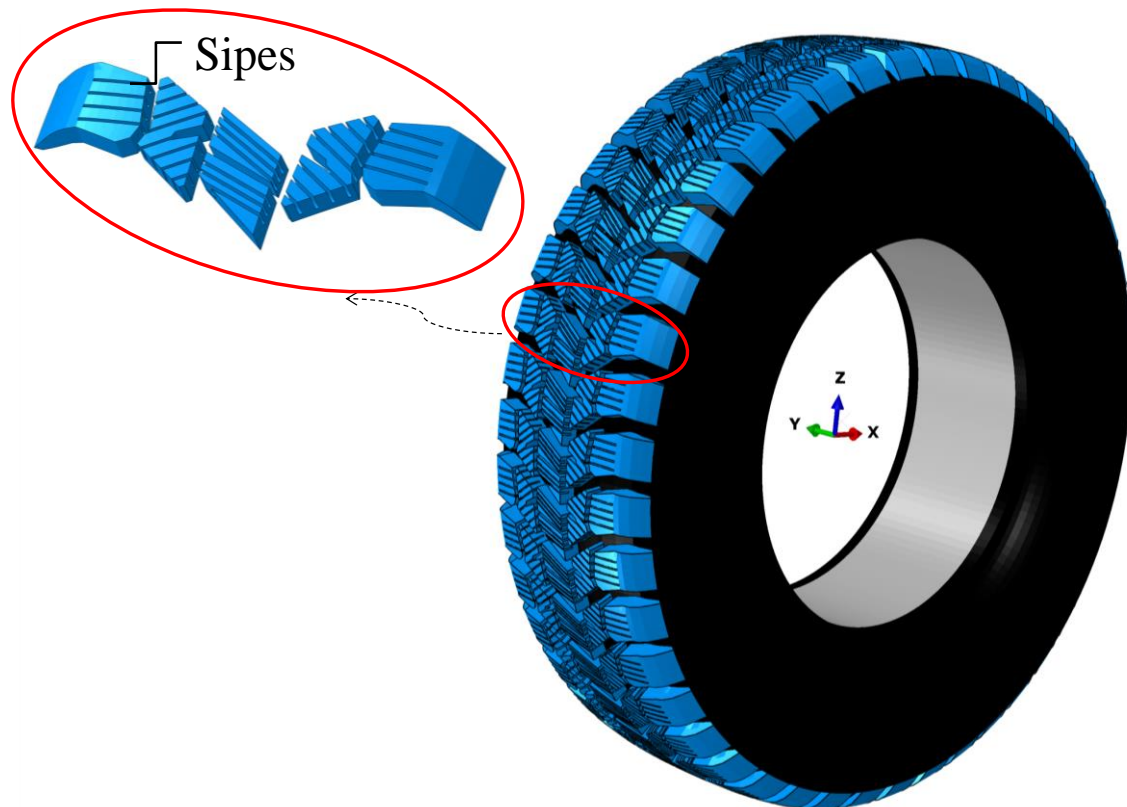


Figure 1.2: Block patterned tread tyre with sipes

1.2 RESEARCH BACKGROUND

The research background section provides a detailed report on all the studies, which were focused on the tyre-snow interaction modeling. A schematic of the literature review is given in Figure 1.3. Shapiro *et al.* (1997) reviewed and compiled a detailed explanation on snow mechanics. Brown (1989) raised the concern on the properties of snow. They vary with density and metamorphism and hence, the degree of confidence

in using these material properties remains less. Voitkovsky *et al.* (1975) showed that the snow with similar densities have different cohesion stress values. This indicates that the microstructure of snow is an essential parameter to obtain mechanical properties. Snow has internal bonding between its ice crystals (Fierz *et al.* 2009). The internal bonding along with grain size and grain shape has a significant influence on snow mechanical properties than the density alone. Such properties of snow make it different from sand. Japan tried to apply Switzerland's guidelines to construct an avalanche control structure. Katakawa *et al.* (1992) showed that even though both countries have the same density of snow, the pressure distribution in avalanche control structure of the former was 1.7 times higher than the latter. Hence, to model snow of a particular country, parameters must be selected from experiments conducted on snow from the same country or snow microstructure should be similar.

Because of above stated reasons, initial studies were widely focused on outdoor tests. However those tests were restricted by region and season. To overcome these predicaments in outdoor tests, researchers have adopted numerical methods. As Brown (1989) stated, those properties of snow are uncertain in nature. This complexity in numerical tyre-snow interaction analysis leads to the qualitative argument over tyre performance in snow terrain.

Over the years, snow has been modeled as elastic (Smith 1972), nonlinear elastic (Smith and Curtis 1975), viscoelastic (Lang and Sommerfeld 1977), elastic-viscoplastic (Cresseri and Jommi 2005) and elasto-plastic (Meschke, Payer, and Mang 1997). Recently, researchers have been widely using modified Drucker-Prager Cap model to simulate tyre-snow interaction (Haehnel and Shoop 2004; Lee 2009; Shoop 2001). Tyre-snow interaction analysis has been extended to three dimensions by Shoop (2001). In these literature, the terrain has been modeled in Finite Element (FE) and block patterned tread has not been taken into account.

Seta *et al.* (2003) and Choi *et al.* (2012) used Coupled Lagrangian Eulerian (CEL) method to model block patterned tread tyre-snow interaction and captured rut formation. Though they obtained force-time characteristics, the detailed effects of sipes and force-torque relations have not been included. Lee (2009) has identified three deformation zones for pressure–sinkage of snow, (i) A small elastic zone, (ii) A propagating plastic zone and (iii) A densification zone. Lee (2011) has also implemented a procedure to obtain force-slip characteristics in FEM by using a

smooth tyre. In these literature, the importance of sipes has not been discussed. Nakajima (2003) implemented an analytical model to estimate the tyre traction in snow. However, the author has assumed rectangular contact area and groove area in tread pattern which makes the model invalid for complex tread pattern.

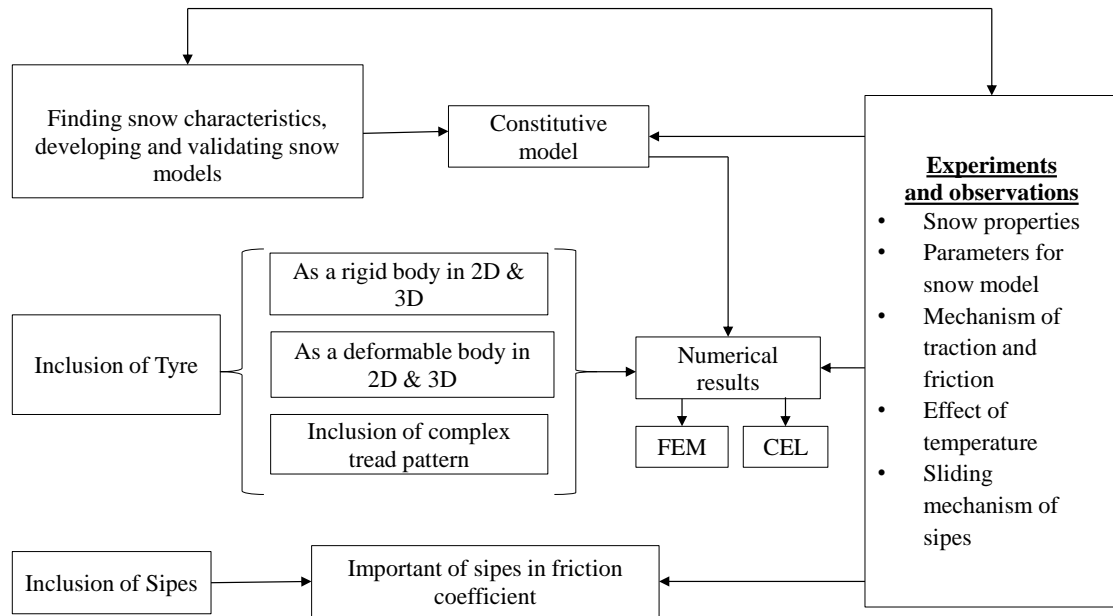


Figure 1.3: A schematic of Literature review

Ella *et al.* (2013), Ripka *et al.* (2012) and Giessler *et al.* (2010) have extensively studied the rubber friction on snow for tyres. The frictional energy in contact area melts the snow and creates a thin water layer between tyre and snow and this reduces the solid to solid contact (Ella *et al.* 2013, Giessler *et al.* 2010 and Ripka *et al.* 2012). Sipes play a significant role by clearing water in the contact area and re-establish solid to solid contact between tyre and snow. This mechanism is called ploughing (Ella *et al.* 2013). As the tyre sipes dig into snow terrain, contact zone cools. This cooling reduces the tyre surface temperature and leads to less heat energy (Giessler *et al.* 2010). Owing to the stated reasons, tread with sipes shows higher coefficient friction than smooth cap (Ella *et al.* 2013).

1.3 MOTIVATION

Based on the literature survey, gaps were identified in the field of numerical tyre-snow interaction. An alternate numerical method is needed to capture rut formation better than that from FEM and CEL. The effect of sipes and tread on force characteristics of tyre-snow interaction needs to be obtained for various tyre profiles.

Capturing rut formation is an essential task to understand the snow tyre traction mechanism. The snow beneath the tyre undergoes large deformation so that in Lagrangian and updated Lagrangian methods have difficulties in contact penetration, element distortion and free surface formation. To capture better rut formation, a mesh free Material Point Method (MPM) is needed.

1.4 SMOOTHED PARTICLE HYDRODYNAMICS (SPH)

A classical MPM is Smoothed Particle Hydrodynamics (SPH). SPH method is a particle-based method which was developed to solve astrophysical problems. In this method, the computational domain is represented by a set of particles. Originally, SPH method was independently invented by Joe Monaghan, Bob Gingold (1977) and Leon Lucy (1977) in 1977. In SPH, properties are assigned to each particle and these particles are capable of moving in a three-dimensional space. There are two steps in obtaining SPH formulation.

(i) Kernel approximation

(ii) Particle approximation

1.4.1 Kernel Approximation

In FEM, elements are connected by nodes whereas in SPH method, the particles are connected by a smoothing function called Kernel function. The function value can be represented in integral form as,

$$A(x) = \int_{\Omega} A(x') \delta(x - x') d\Omega \quad (1.1)$$

where, A is a function of position vector, x is a three-dimensional position vector, $\delta(x - x')$ is a Dirac delta function and Ω is volume.

$$\delta(x - x') = \begin{cases} 1, & x = x' \\ 0, & x \neq x' \end{cases} \quad (1.2)$$

When $x = x'$, the integral is exact but it is a point function and cannot be used to implement numerical method. If we can replace the Dirac delta function with the kernel approximation function $w(x - x', h)$, then the kernel approximation of $A(x)$ becomes,

$$A(x) \approx \int_{\Omega} A(x')w(x-x',h)d\Omega \quad (1.3)$$

where h is a smoothing length which represents the influence length for each particle. Note that Smoothing function is an approximate function of Dirac delta function. So the integral representation with smoothing function is an approximation of the exact solution. The design of smoothing function is such that as h approaches zero, it becomes Dirac delta function. The derivative of a function can also serve as function approximation. At the end, the kernel approximation of derivative can be written as (Liu and Liu 2010, Eqn. 15),

$$(A(x))' \approx -\int_{\Omega} A(x')(w(x-x',h))'d\Omega \quad (1.4)$$

1.4.2 Particle Approximation

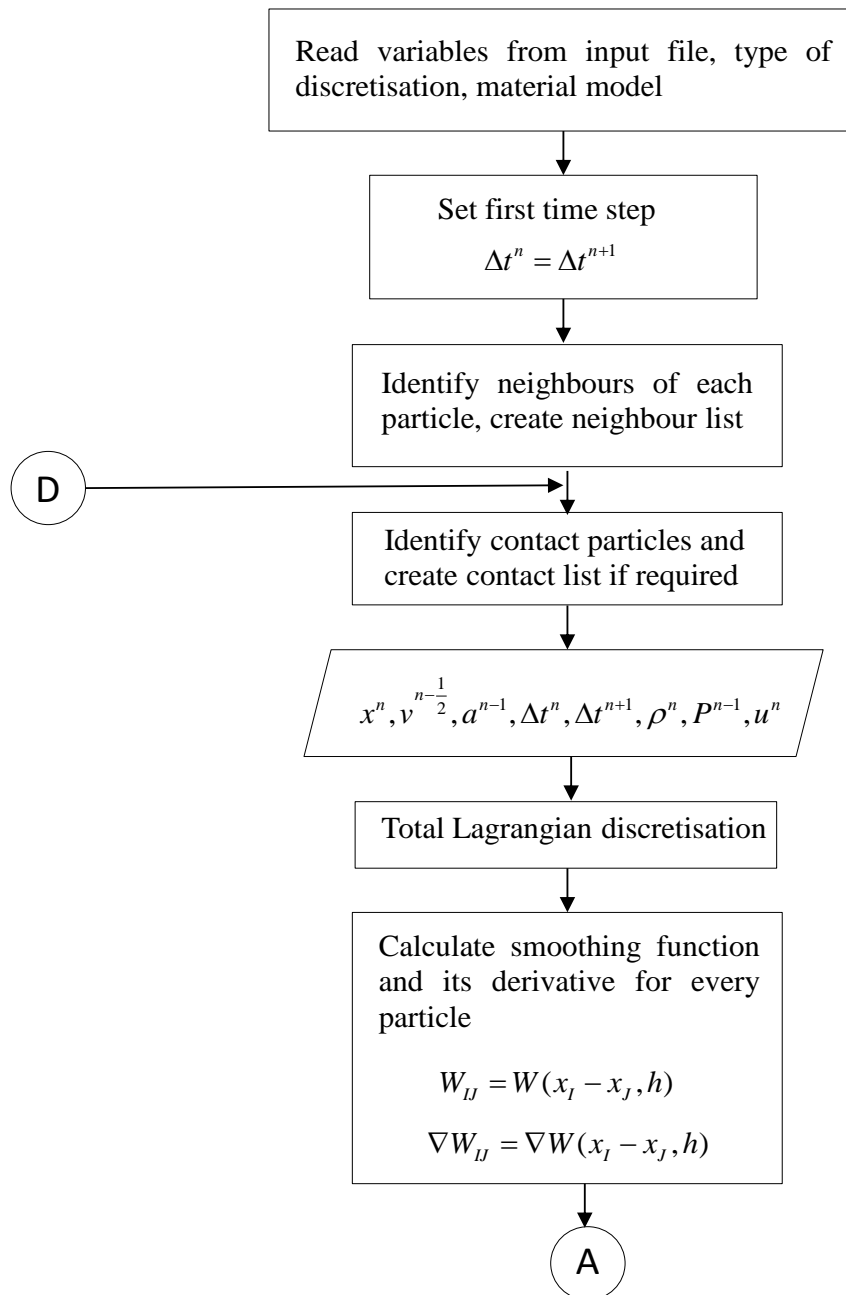
This step involves converting integral representation to particle representation then estimating the field variable on particles present in the problem domain. These particles also represent the material points with, density and mass. Based on the distance between particles and the total volume, a lumped volume can be assigned to each particle. The continuous integral representation concerning the SPH kernel approximation can be converted into a discretized form of summation over the entire particles within the influence domain. This process is commonly known as particle approximation. The infinitesimal volume $d\Omega$ in kernel approximation is replaced by a finite volume of the particle. This finite volume is replaced with the corresponding mass to density ratio. So the particle approximation can be written as,

$$A(x) \approx \sum_{j=1}^N \frac{m_j}{\rho_j} A(x_j)w(x-x_j,h) \quad (1.5)$$

where, N is the total number particles within the influence length. By following the same procedure, particle approximation of derivatives can be obtained. This particle approximation makes SPH method a mesh free method.

1.4.3 Total Lagrangian Formulation for SPH

Reveles (2007) explained a detailed implementation of SPH method in the total lagrangian formulation. The explanation is given in Figure 1.4 (Reveles 2007, Fig. 5.2).



A

Carry out pull back operation
on particle position

$$u^{n-\frac{1}{2}} = u^n - \frac{1}{2}v^{n-\frac{1}{2}}\Delta t^n$$

Calculate deformation gradient for every particle

$$\langle F_I \rangle = -\sum_{J \in S} (u_J - u_I) \otimes \nabla_{X_J^0} W(X_I - X_J, h_0) V_J^0 + I$$

Calculate rate of deformation gradient for every
particle

$$\langle \dot{F}_I \rangle = -\sum_{J \in S} (v_J - v_I) \otimes \nabla_{X_J^0} W(X_I - X_J, h_0) V_J^0$$

Carry out push forward
operation on particle position

$$u^n = u^{n-\frac{1}{2}} + \frac{1}{2}v^{n-\frac{1}{2}}\Delta t^n$$

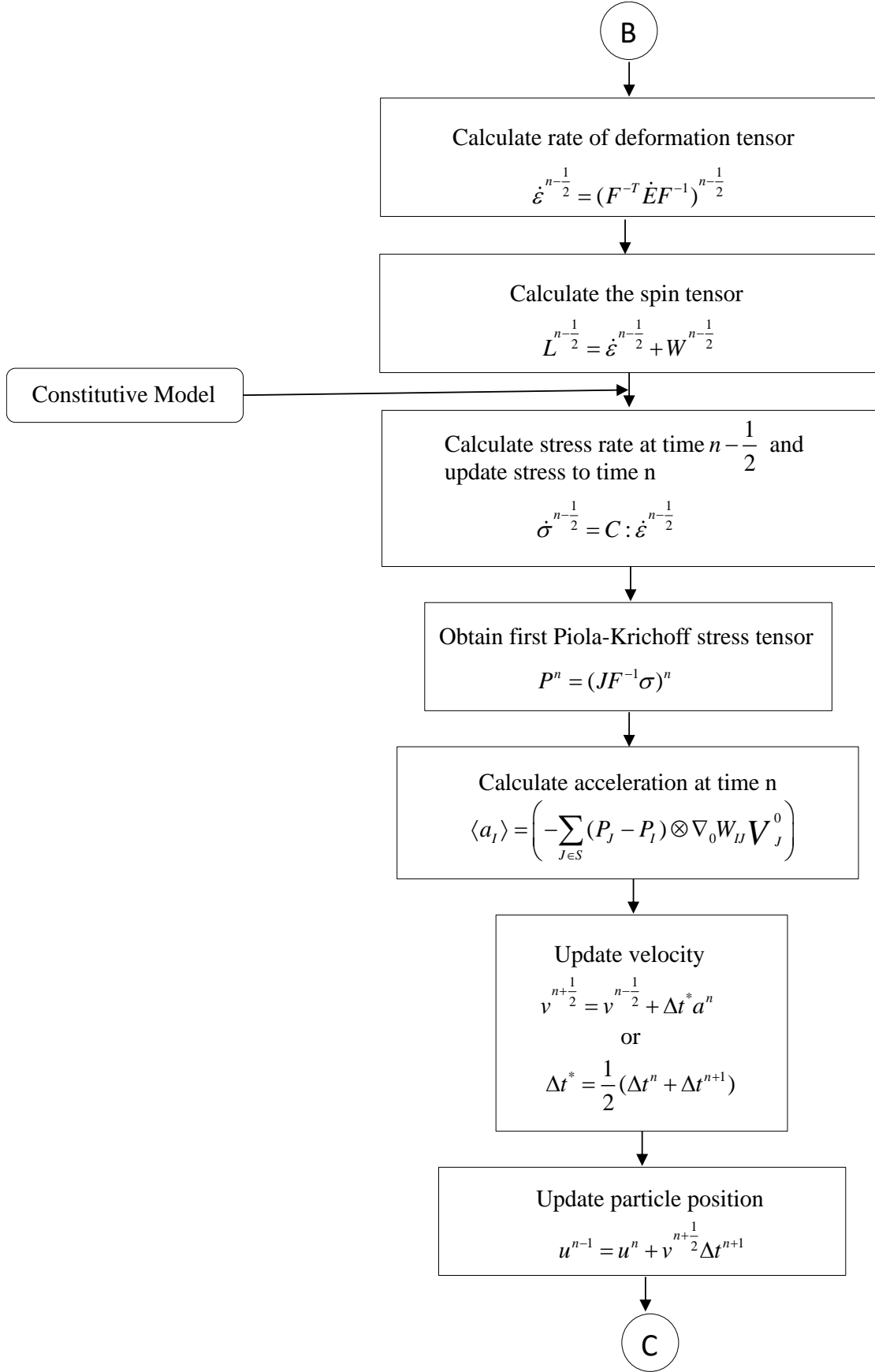
Obtain Jacobian and update
all particle densities

$$J = \det |F^n|$$
$$\rho_J^{n+1} = J^{-1} \rho_{0J}$$

Obtain time rate of Green-Lagrange strain tensor

$$\dot{E}^{n-\frac{1}{2}}(X_i) = \frac{1}{2}(\dot{F}^T F + F^T \dot{F})^{n-\frac{1}{2}}$$

B



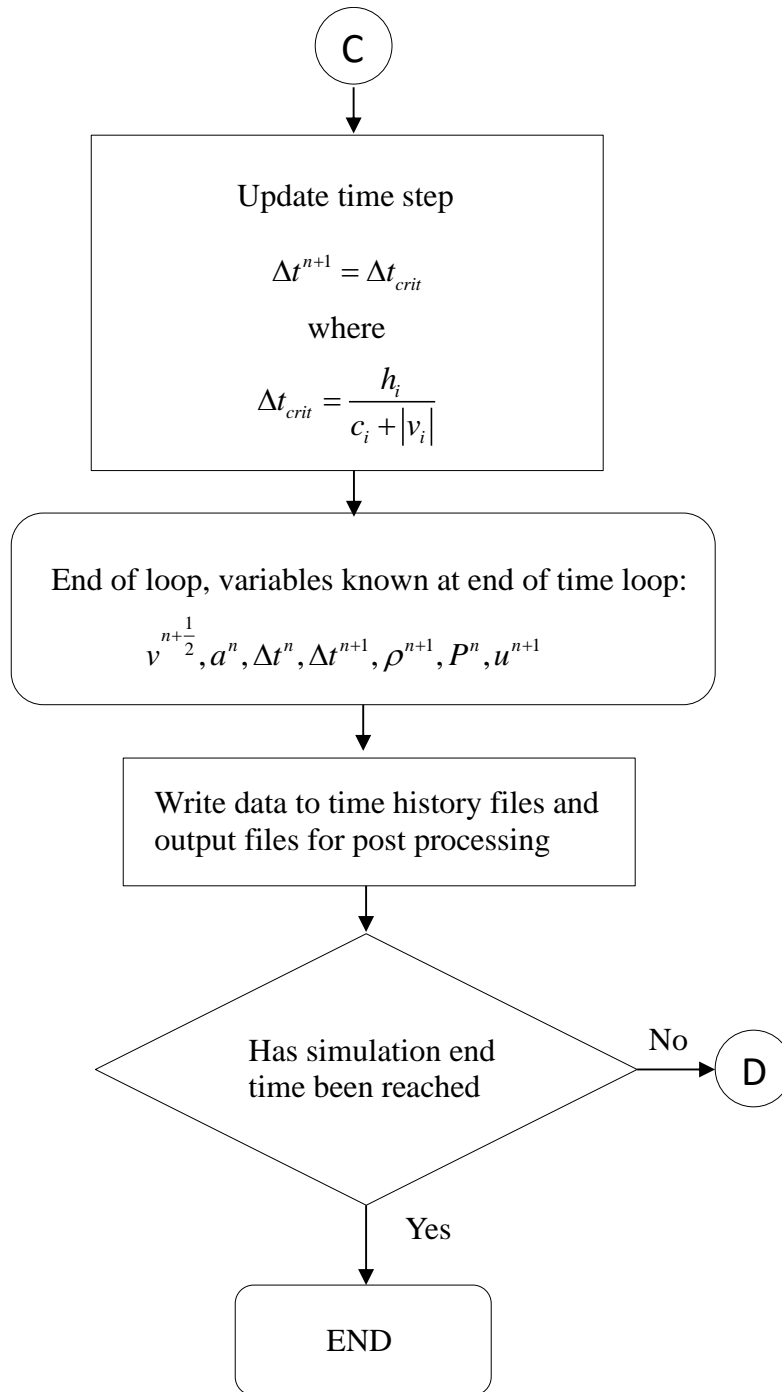


Figure 1.4: A schematic of implementation of SPH in Total Lagrangian formulation

(Source: Reveles, 2007, Fig. 5.2)

Bui *et al.* (2008) pointed out that SPH particles behave like atoms in solids. When solid get compressed, atom repels each other as it attracts under tension. This attraction in SPH particles during large tension make them group together and form clumps. This numerical problem in SPH method is known as tensile instability. Researchers have attempted to solve this problem by assigning a small repulsive force

between particles (Monaghan 2000 and Gray *et al.* 2001). Yet, the application of SPH method to solve large tension in solid is less. In tyre-snow interaction analysis, snow beneath the tyre is under compression by the application of vehicle load. Hence, the numerical tensile instability will not occur in tyre-snow interaction analysis. Lescoc (2010) and Dhillon (2013) used the coupled FEM-SPH method for tyre-soil interaction. Tyre was modeled using FEM and soil was modeled using SPH. Both the authors have studied the effect of soil ahead of the rolling tyre on motion resistance.

1.5 MODIFIED DRUCKER-PRAGER CAP MODEL

In this study, the Modified Drucker-Prager Cap (MDPC) model has been used to model snow. MDPC model is an elasto-plastic model which defines a mathematical boundary to separate elastic and plastic regions. MDPC models' yield surface consists of a shear failure region, a transition surface and a cap region as show in Figure 1.5. In SIMULIA/Abaqus documentation (SIMULIA Inc. 2014), the MDPC model has been explained in the material section.

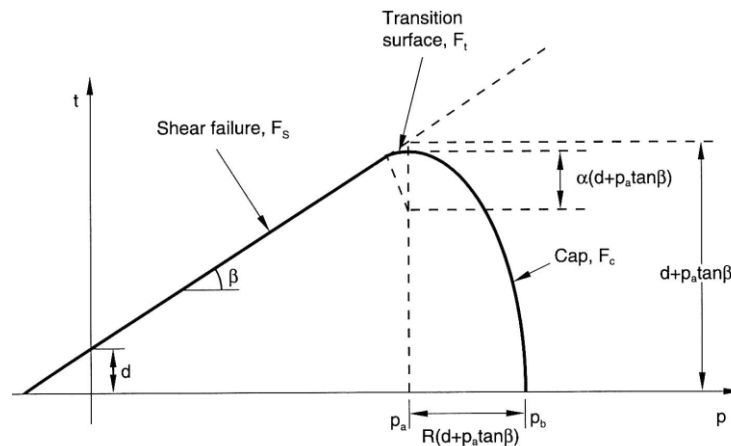


Figure 1.5: The yield surface of Modified Drucker-Prager Cap model in meridional plane

(Source: SIMULIA Inc. 2014, Fig. 23.3.2-1)

The pressure-deviatoric stress plane is called meridional plane. The Drucker-Prager shear failure region is a perfectly plastic yield surface with no hardening. The cap region is used to define an inelastic hardening or softening to capture plastic compaction by expanding or contracting. The transition surface provides a smooth transition between shear and cap regions. The hardening or softening behaviour for

cap region can be defined using pressure-plastic volumetric strain relationship using experimental data as shown in Figure 1.6.

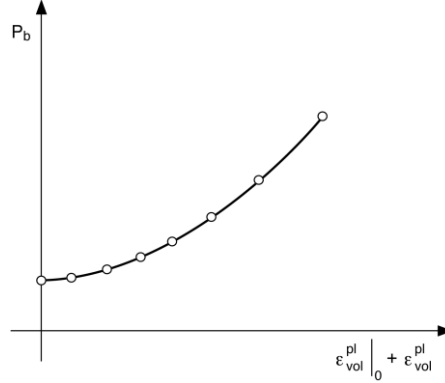


Figure 1.6: The pressure-plastic volumetric strain relationship

(Source: SIMULIA Inc. 2014, Fig. 23.3.2-3)

A linear elastic model is used to define the elastic behaviour. The Drucker-Prager shear failure surface is given as,

$$F_s = t - p \tan \beta - d = 0 \quad (1.6)$$

where, β is friction angle, d is cohesion stress value, p is hydrostatic pressure and the deviatoric stress t is written as,

$$t = \frac{1}{2} q \left[1 + \frac{1}{K} - \left(1 - \frac{1}{K} \right) \left(\frac{r}{q} \right)^3 \right] \quad (1.7)$$

Here, q is von-mises equivalent stress, r is third invariant of stress tensor and K is a material parameter which is used control the stress values in tension and compression as shown in Figure 1.7. In ABAQUS/Explicit, the only option available is $K=1$.

The transition surface between shear and cap region is written as,

$$F_t = \sqrt{(p - p_a)^2 + \left[t - \left(1 - \frac{\alpha}{\cos \beta} \right) (d + p_a \tan \beta) \right]^2} - \alpha (d + p_a \tan \beta) = 0 \quad (1.8)$$

where, α is used to define the smooth intersection between shear failure and cap surfaces and p_a is an evolution parameter for cap surface to capture hardening.

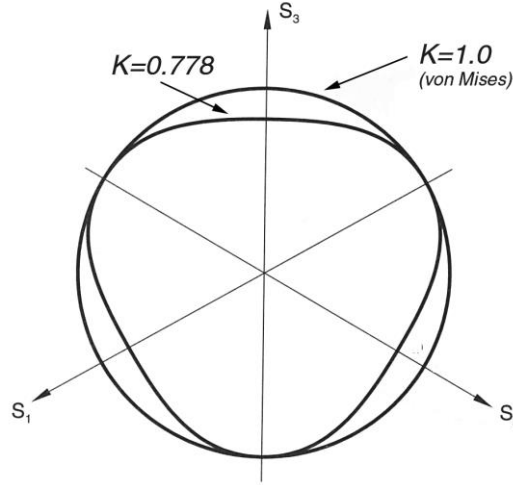


Figure 1.7: The yield surface of Modified Drucker-Prager Cap model in deviatoric plane

(Source: SIMULIA Inc. 2014, Fig. 23.3.2-2)

The cap yield surface is defined as,

$$F_C = \sqrt{(p - p_a)^2 + \left[\frac{Rt}{(1 + \alpha - \alpha / \cos \beta)} \right]^2} - R(d + p_a \tan \beta) = 0 \quad (1.9)$$

Here, R is a material parameter to control the cap surface shape.

The plastic flow of the deformation is defined by the plastic flow potential. The plastic flow rule is divided into two types as follows,

- (i) Associated flow rule – The yield surface and the flow potential are identical. This gives the deformation at a right angle to the yield surface.
- (ii) Non-associated flow rule – A unique equation is used for flow potential. This gives the deformation at an angle to the yield surface.

In MDPC model, the shear failure region and the transition region are employed with non-associated flow rule and the cap region is defined with associative flow rule.

Hence, the plastic flow potential for shear failure region and transition region is expressed as,

$$G_s = \sqrt{\left[(p_a - p) \tan \beta \right]^2 + \left[\frac{t}{(1 + \alpha - \alpha / \cos \beta)} \right]^2} \quad (1.10)$$

For cap region, the plastic flow potential is cap yield surface and given in Equation (1.9). The plastic flow potentials formed a smooth continuous profile as seen in Figure 1.8.

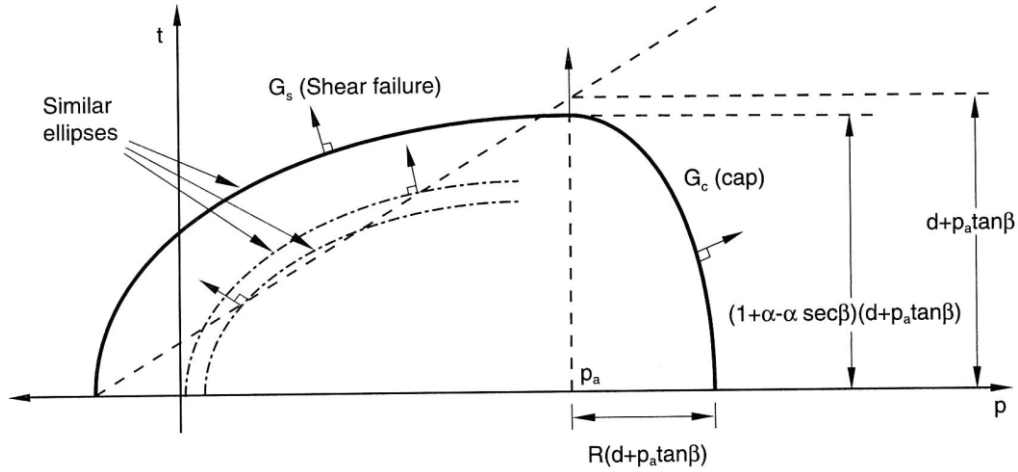


Figure 1.8: The plastic flow potential in meridional plane

(Source: SIMULIA Inc. 2014, Fig. 23.3.2-4)

The parameters to model snow has been obtained from literature (Haehnel *et al.* 2004) and presented in Chapter 3.

1.6 SPONGE EFFECT

When a tyre is loaded on soft snow, the entire load is supported by the compression of snow particles beneath the tyre. Snow particles act independently to support the vehicle load and the particles which are away from the loaded area are not affected, as shown in Figure 1.9.

However, Figure 1.10(a) and Figure 1.10(b) indicate that the Lagrangian and CEL snow models act as a single unit when subjected to a compressive vehicle load and this load is largely supported by the tension between elements near sidewall area. This effect is known as sponge effect (Lescoe 2010 and Dhillon 2013).



Figure 1.9: Natural snow behavior under vehicle load

(Source: https://en.wikipedia.org/wiki/Snow_tire)

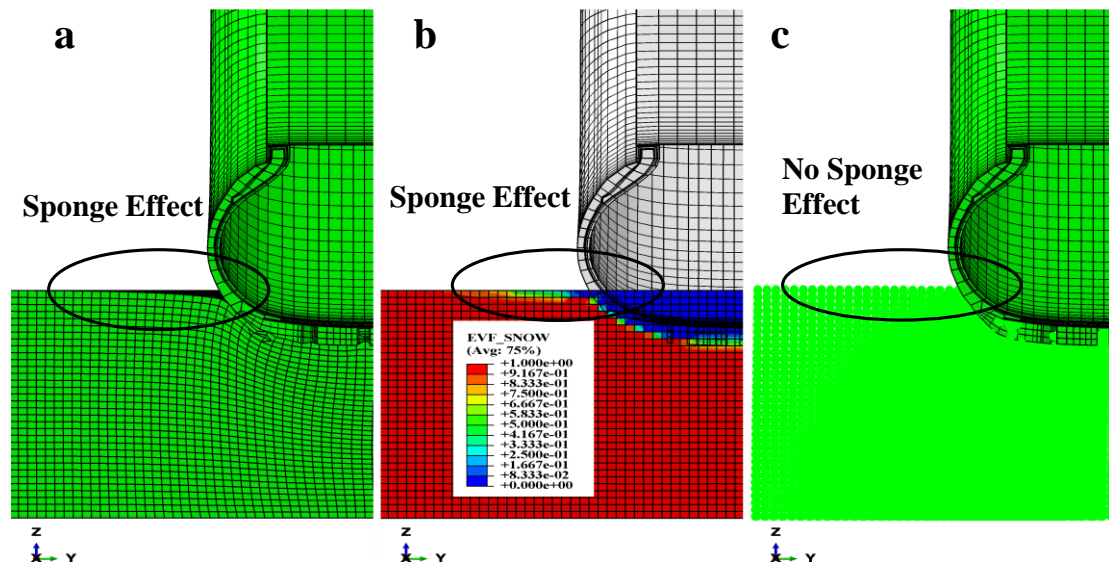


Figure 1.10: Cut section of a loaded tyre on (a) Lagrangian (b) CEL with EVF contour and on (c) SPH snow blocks

In the Eulerian method, material moves independent of mesh. To show snow deformation, Element Volume Fraction (EVF) contour has been taken in Figure 1.10(b). EVF equal to one corresponds to 100% material in the element and zero

corresponds to null. Sponge effect is not a natural phenomenon of snow behavior under compression. However in SPH snow model, as seen from Figure 1.10(c), vehicle load is generally supported by the compression of particles and there is a lack of sponge effect near the sidewall. This matches well with natural snow compression.

1.7 OBJECTIVE AND SCOPE OF THE RESEARCH

Shear failure of snow in the groove area of tread pattern is an important factor in longitudinal traction and this will be discussed later in the mechanism of tyre traction in snow. But the shearing of elements in FEM creates issues such as element distortion, element deletion and convergence problems.

Most of the available research on tyre-snow interactions use smooth cap tyre for analysis due to restrictions in FEM technique. In this present work,

- The mechanism of tyre traction in snow terrain is explained in detail.
- To overcome the restrictions of FEM on tyre-snow interaction analysis, a new method is needed. Three different numerical methods (FEM, CEL and SPH) have been compared to model tyre-snow interaction.
- Frictional energy in contact area melts snow and creates a water layer (Ella *et al.*, 2013). Sipes bend and remove water layer from the contact area, because of the channel effect. This turns a part of the problem into a hydroplaning. Three different tread patterns (smooth cap, block patterned tread and block patterned tread with sipe) have been compared for critical velocity in hydroplaning. Owing to the water removal capacity of sipes, tread with sipes has a higher coefficient of friction than that without sipes. A numerical procedure has been implemented to find the difference in friction coefficient using single tread block with and without sipes.
- A numerical procedure has been implemented to obtain longitudinal slip-force characteristics.
- The variation of traction and motion resistance with respect to torque is obtained for various cases such as a smooth tyre, a block patterned tread tyre with and without sipes for soft and hard snow with various loads.

1.8 ORGANISATION OF THE THESIS

The work on the longitudinal characteristics of snow tyres using coupled FEM-SPH method is explained in the following chapters.

Chapter 2 explains the mechanism of tyre traction in snow. The effects of undistributed snow ahead of rolling tyre, tyre sinking depth and traction have been explained in detail.

In Chapter 3, FEM, CEL and SPH methods have been compared to model tyre-snow interaction using plate-sinkage test, tyre indentation test and tread indentation test.

Chapter 4 captures the importance of sipes in snow tyres. The smooth cap tyre, block patterned tread tyres with and without sipes have been compared for critical velocity of hydroplaning. The numerical experiments have been conducted to capture the difference in friction coefficient of rubber blocks with and without sipes.

Chapter 5 explains the procedure to obtain longitudinal slip-force characteristics and it answers, whether the longitudinal slip-force curve is suitable for snow tyres or not.

Chapter 6 gives the variation of traction and motion resistance with respect to torque is obtained for various cases such as a smooth tyre, a block patterned tread tyre with and without sipes for soft and hard snow with various loads.

Chapter 7 summarizes the conclusion of this present work in the field of numerical tyre-snow interaction and the scope of future research.

CHAPTER 2

THE MECHANISM OF TYRE TRACTION IN SNOW

2.1 FORCES ACT ON TYRE

The fundamental forces due to tyre-snow interaction was identified by Browne (1974). The authors has adopted and advanced Browne's tyre-snow traction mechanism. Figure 2.1 represents the forces act on tyre when it rolls over an uncompact snow terrain. Five forces, as shown in Figure 2.1, act in tyre-snow interaction.

- (i) Motion resistance Force, F_1
- (ii) Force due to compressed snow in groove, F_2
- (iii) Traction force, F_3
- (iv) Vertical force due to contact pressure, F_4
- (v) Rolling resistance Force, F_5

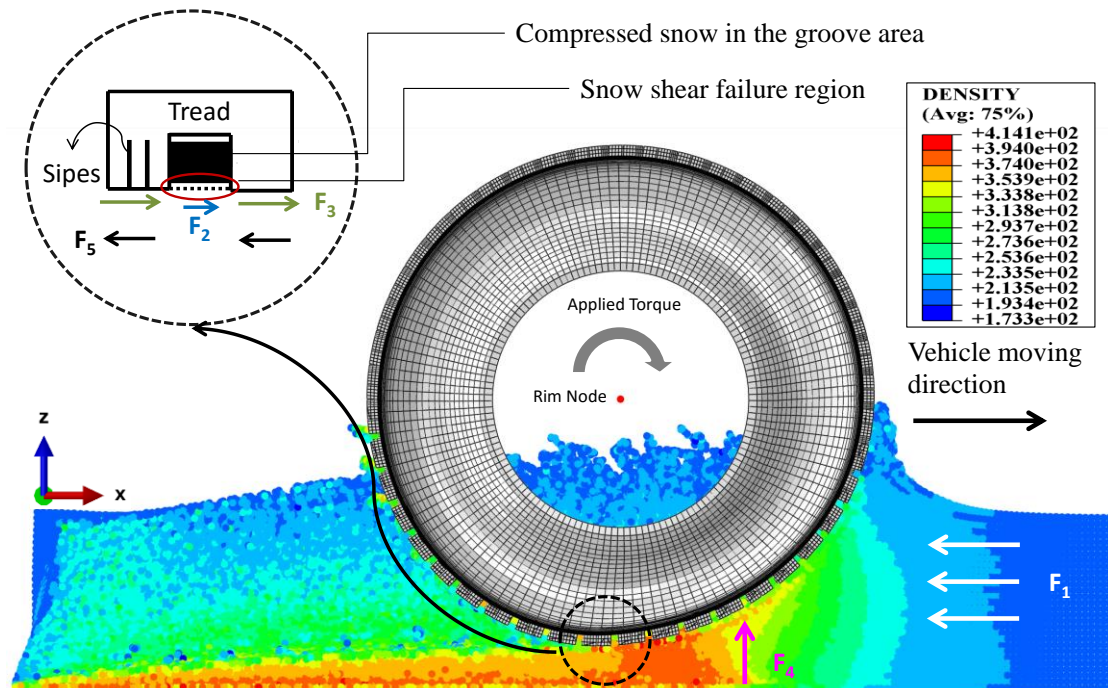


Figure 2.1: Cut section of tyre-snow interaction shows forces act on the tyre

2.1.1 Motion Resistance Force

Snow is a nonlinear natural material which undergoes large deformation under the application of load. The snow beneath the tyre is compressed by the vehicle load and snow ahead of rolling tyre acts as a resistance to motion as shown in Figure 2.1. This resistance force is called Motion Resistance Force (MRF), F_1 .

2.1.2 Force due to Compressed Snow in Grooves

During loading, snow is compressed into the grooves of the tread pattern. This increases the shear strength of the snow which is trapped inside the grooves. When the tyre accelerates, the wheel spinning speed ($r\omega$) is greater than forward vehicle speed (v_x). This speed difference causes the sliding velocity at the top of tread. However, the presence of compressed snow in the groove creates a gear effect which resists the tread deformation and holds higher torque value. The lack of tread deformation causes the compressed snow to hold the torque and produces a force due to contact pressure. The sum of these forces is represented as F_2 in Figure 2.1. When the force due to applied torque overcomes the shear strength, blocks of compressed snow fail at the region shown in Figure 2.1 and resistance becomes zero. This snow shear resistance is absent in tyre with the smooth cap pattern. Shear failure of compacted snow indicates that the tyre with block patterned tread can hold higher torque or higher slip than the tyre with a smooth cap.

2.1.3 Traction Force

Slip occurs at contact patch due to velocity difference between the forward vehicle speed and the wheel spinning speed (Pacejka 2006). This mechanism can be explained using tyre brush model (Pacejka 2006). The tread is assumed as elastic bristles in tyre brush model. In free rolling condition, the bristles are compressed in vertical direction without producing any horizontal deformation. However in acceleration, the wheel spinning speed is greater than the forward vehicle speed and creates a horizontal deformation. The force developed due to this horizontal deformation is called traction force, F_3 as shown Figure 2.1.

2.1.4 Rolling Resistance Force

The presence of hysteresis in viscoelastic material creates Rolling Resistance Moment (RRM) which opposes vehicle motion in acceleration.

Figure 2.2 shows that the deformation of a rolling tyre on road is symmetric (when viscoelasticity is neglected) about the origin, but in snow the tyre deformation leans towards the leading edge due to sinking in snow, creating a shift towards leading edge in vertical force due to contact pressure as shown in Figure 2.2 and represented in Figure 2.1 as F_4 .

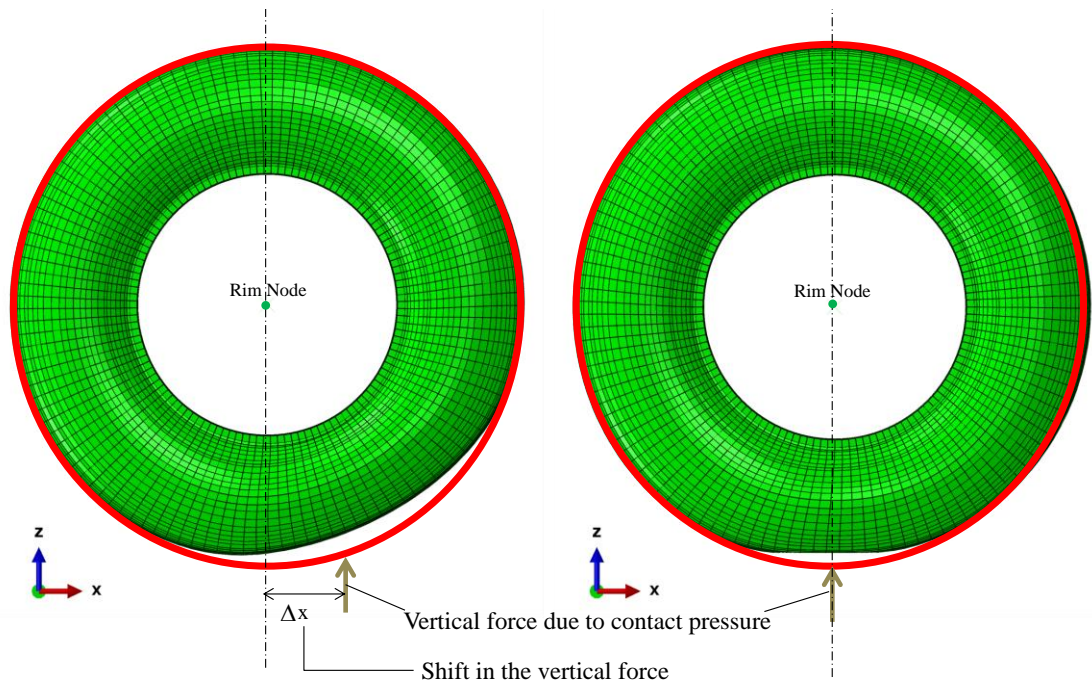


Figure 2.2: Deformed shape of the rolling tyre on snow (left) and on road (right) with the undeformed shape shown in red outline

This deformation of the tyre in snow is a function of load, velocity, inflation pressure, snow depth and snow cohesion. There is a shift in vertical force by a distance Δx causing an additional RRM, responsible for a Rolling Resistance Force (RRF), F_5 in the opposing direction of vehicle motion as shown in Figure 2.1.

2.2 SUMMARY

The effect of sipe is an important factor of tyre traction in snow. Frictional energy in contact area melts snow and creates a water layer between tyre and snow. This reduces the solid to solid contact and reduces friction. During rolling, Sipes bend and remove water layer from contact region to re-establish solid to solid contact and increases the friction coefficient. The rubber used in the snow tyre tread compound has low glass transition temperature than summer tyre to maintain the viscoelastic property at low temperature.

The drawbar pull that acts on the tyre is the algebraic sum of traction, MRF, force due to compressed snow in grooves and RRF. The longitudinal component of contact force that acts on tyre is the algebraic sum of MRF and force due to compressed snow in grooves. In this study, acceleration condition is used for all analyses. The following terminologies are used in this work to understand the mechanism of tyre-snow interaction.

$$\text{Drawbar pull acting on tyre during acceleration} = (F_2 + F_3 - F_1 - F_5) \quad (2.1)$$

$$\text{Net longitudinal force due to contact pressure} = -F_1 + F_2 \quad (2.2)$$

In acceleration condition, MRF and RRF have a negative impact on acceleration and during brake condition, these contribute for braking. At higher slip ratios, the effect of shear failure at contact region has a minimal effect on drawbar pull acting on tyre but the effect of sipes exists in all slip ratios.

CHAPTER 3

COMPARISON OF FEM, CEL AND SPH NUMERICAL METHODS

3.1 INTRODUCTION

Lagrangian and updated Lagrangian methods have difficulties in contact penetration, element distortion and free surface formation. Shoop (2001) showed that the FEM snow model underestimates the deformation. As explained in the Introduction section, to overcome the restrictions of FEM in snow modeling and for better prediction of snow deformation, an efficient numerical method needs to be identified. In this work, three numerical methods are compared for, plate-sinkage test, tyre indentation test and tread indentation test have been made.

3.2 PLATE-SINKAGE TEST

Laboratory experimental data is chosen from the literature (Haehnel and Shoop 2004). In the laboratory test, 0.23 m diameter rigid plate was pushed into a slab of snow $0.6 \times 0.6 \times 0.5 \text{ m}^3$ with an average initial density of 180 kg/m^3 . A load of 1867 N was applied on the plate and the deformation of snow surface at the end of the applied load was 0.2 m.

The same laboratory condition has been implemented in ABAQUS/Explicit environment. The plate is modeled using Lagrangian method and snow is modeled separately using the following three methods: Lagrangian, CEL and SPH. Plate is assumed as linear elastic and snow is modeled as elasto-plastic (modified Drucker-Prager Cap model). Properties of snow model have been taken from the literature (Haehnel and Shoop 2004) and presented in Table 3.1 and Table 3.2. The modeling procedure to create SPH snow in ABAQUS is explained in Appendix A.

Table 3.1: Parameters for Modified Drucker-Prager Cap model

Parameter	Values
Initial density, ρ	180 (kg/m^3)
Young's modulus, E	13.790×10^6 (N/m^2)
Poisson's ratio, ν	0.3
Drucker-Prager cohesion, d	5000 (N/m^2)
Drucker-Prager friction angle, β	22.538 (deg)
Cap eccentricity, R	0.02
Initial cap yield surface position, $\mathcal{E}_{vol}^{pl} _0$	0.001
Transition surface parameter, α	0
Flow stress ratio, K	1

Snow is modeled using uniform node density of 10 mm between nodes in all numerical methods. Snow top surface has been left free and all other sides and bottom have been constrained normal to the surface in FEM and CEL methods. SPH snow is constrained by a rigid top open box around it. The rigid box constrained snow particles in the normal direction. The friction between snow and plate is taken as 0.3 (Haehnel and Shoop 2004; Shoop 2001). In SPH method, quadratic, cubic and quintic kernel functions have been compared. Table 3.3 shows that the prediction of vertical displacement of the plate in the snow using SPH with cubic kernel function matches closely with the experimental displacement. Lagrangian and CEL methods underestimate and SPH with quadratic and quintic kernel functions overestimates the vertical displacement.

Table 3.2: Hardening law

Hydrostatic Pressure (N/m^2)	Volumetric Plastic Strain
113.76	0
5.00×10^4	0.593
1.00×10^5	0.669
2.00×10^5	0.806
5.00×10^5	0.944
1.00×10^6	1.083
2.00×10^6	1.299
2.80×10^6	1.455
3.25×10^6	1.475
6.00×10^6	1.5
6.00×10^7	1.514

Table 3.3: Plate-Sinkage comparison with vertical displacement of plate into snow

Analysis	Kernel Function	Plate Displacement (m)
Lagrangian	--	0.159
CEL	--	0.163
SPH	Quadratic	0.219
SPH	Cubic	0.199
SPH	Quintic	0.328

This proves that SPH with cubic kernel function is a better choice to model snow and vertical displacement contour is shown in Figure 3.1(c). CEL analysis calculates field variables using EVF and nodal outputs are not stable as shown in Figure 3.1(b). Element distortion and contact penetration are unavoidable in FEM analysis as seen in Figure 3.1(a).

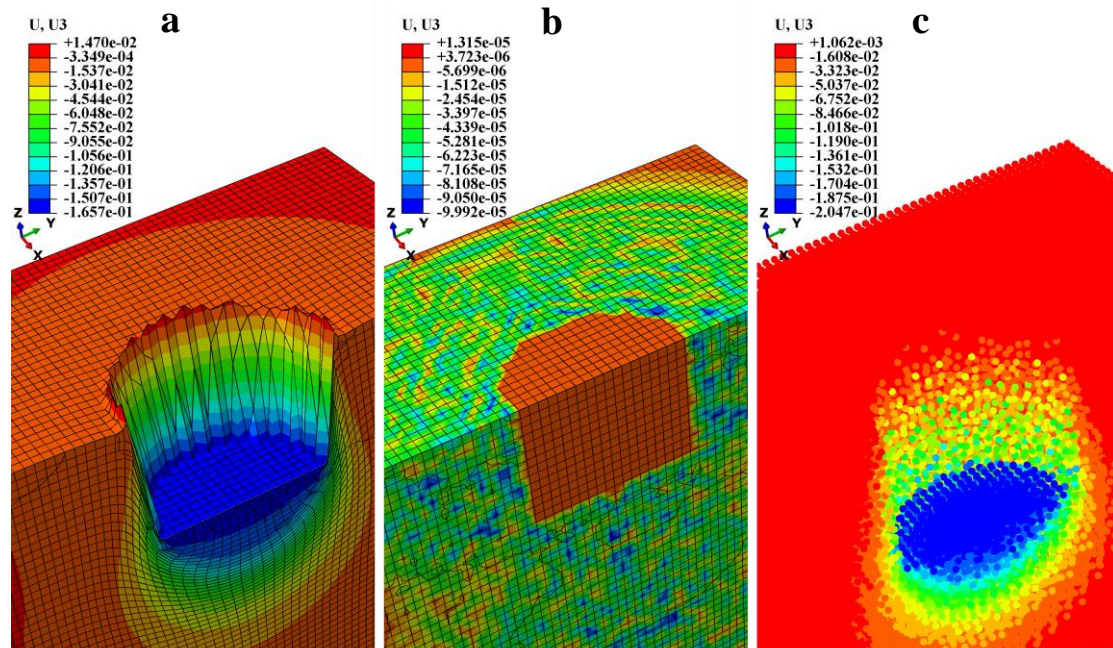


Figure 3.1: Cut section of plate-sinkage analysis using (a) Lagrangian (b) CEL and (c) SPH with cubic kernel function with vertical displacement contours

In subsequent numerical simulations, snow modeled using SPH is employed with cubic kernel function and modified Drucker-Prager Cap model with different cohesion values has been used to create soft and hard snow.

3.3 TYRE INDENTATION TEST

In tyre-snow interaction analysis, capturing rut formation is a crucial aspect to calculate forces acting on tyre. Shear failure in contact region entirely depends on rut formation. In a real situation, during loading, the snow particle enters into the grooves of tyre. Unlike the road, in snow the contact pressure of tyre is distributed over the outer surface of tread, sidewall and inside the groove area. These natural phenomena depend on rut formed by the tyre in snow. In numerical simulations, a method which captures better rut formation can give a better contact pressure distribution. Tyre

indentation tests have been performed to find an appropriate numerical method which can capture better contact pressure distribution.

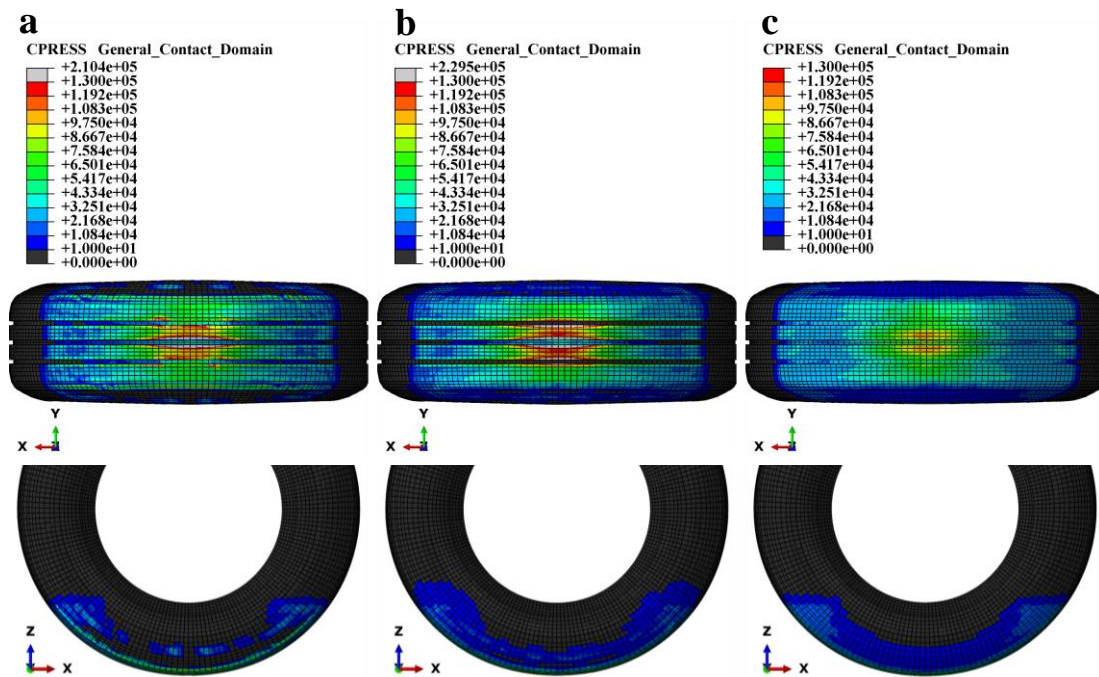


Figure 3.2: Contact pressure (N/m²) of a loaded rib tyre on (a) Lagrangian (b) CEL and on (c) SPH snow box

The FE tyre model used in this study is 235/75R15, has been adopted from Narasimha Rao (2005). The FE tyre model properties and procedure is presented in Chapter 5. Snow is modeled individually using the following three methods: Lagrangian, CEL and SPH. The uniform node density (6 mm between nodes) has been used in all numerical methods. A 210 kPa pressure inflated tyre loaded in a snow box of $0.6 \times 0.6 \times 0.2 \text{ m}^3$ with 4000 N load. The friction coefficient between tyre and snow is assumed as 0.3 based on literature.

The boundary conditions for snow box are the same as used in the Plate-Sinkage test. In Figure 3.2(a) and Figure 3.2(b), the contact pressure at the center of contact patch of rib tyre loaded in Lagrangian and CEL snow boxes shows significantly higher than the tyre loaded in SPH snow box and it has uniform contact pressure than other two as shown in Figure 3.2(c), because of SPH snow entered into the grooves of rib tyre better than other two without contact penetration and element distortion. Table 3.4 shows that the contact area of tyre loaded in SPH snow box is greater than other two due to the stated reasons.

Table 3.4: Contact area of loaded rib tyre in different numerical snow model

Analysis	Contact Area (m^2)
Lagrangian	0.159
CEL	0.189
SPH	0.229

3.4 TREAD INDENTATION TEST

Tread indentation tests have been performed to determine the numerical method that better captures the complex rut formation. Tread is assumed as linear elastic. Snow slab of $0.3 \times 0.2 \times 0.01 \text{ m}^3$ is modeled with the uniform node density (2 mm between nodes).

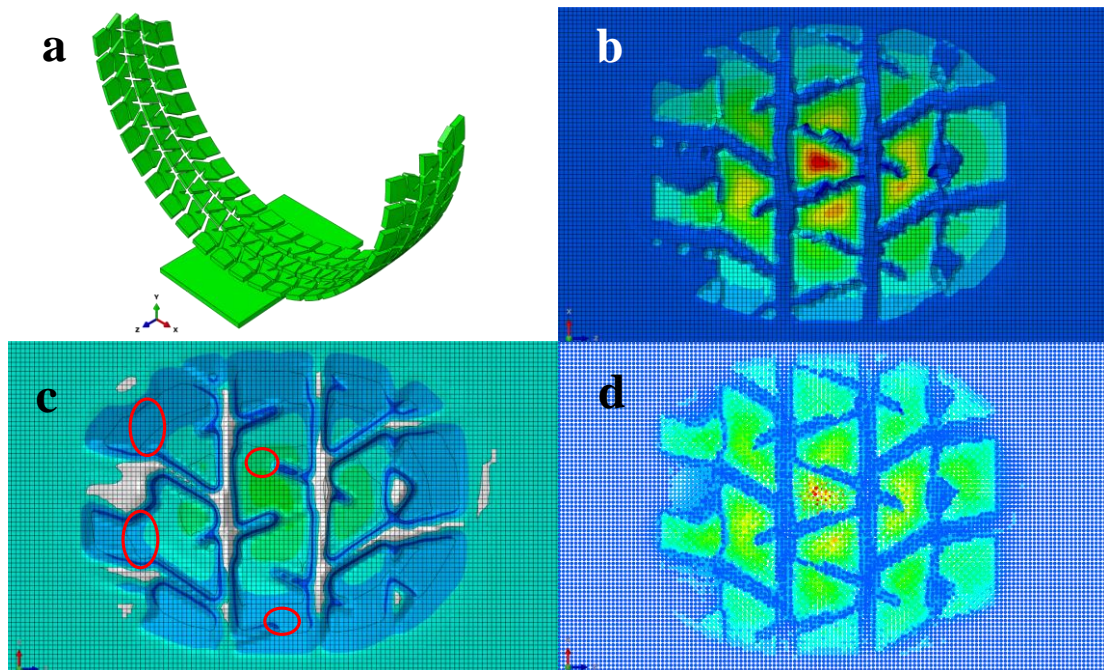


Figure 3.3: (a) Tread-snow assembly and Rut formed by the tread geometry in (b) Lagrangian (c) CEL and on (d) SPH snow blocks.

This has been used in all numerical methods and the tread-snow assembly is shown in Figure 3.3(a). Tread has been pushed 8 mm into snow slab. Snow modeled with Lagrangian method captured rut formation but with the presence of contact

penetration, element distortion and hourglass as shown in Figure 3.3(b). In addition to that, shearing of snow elements cannot be performed in lagrangian method due to material attached to the mesh. The CEL snow model has not captured the complete rut formation due to contact penetration and red outlines indicate the missing rut formation (shown in Figure 3.3(c)). SPH is a mesh free numerical method. Snow modeled using SPH captured the complete rut formation better than other two methods without any contact penetration and element distortion as seen in Figure 3.3(d)

3.5 SUMMARY

Based on the observations from Plate-sinkage test, Tyre indentation test and Tread indentation test, the coupled FEM-SPH method is a better option to simulate tyre-snow interaction analysis without contact penetration and element distortion and with better rut formation. In this study, all tyre-snow interaction analyses have been carried out using the coupled FEM-SPH method. Tyre is modeled using FEM and snow is modeled using SPH.

CHAPTER 4

IMPORTANCE OF SIPES

4.1 INTRODUCTION

Snow melts in the contact region creates a thin water layer due to the frictional energy of rolling tyre. Water layer in the contact region reduces the solid to solid contact between tyre and snow. Sipes in the tread pattern bend and remove the water layer from the contact patch. This water removal process of sipes re-establishes solid to solid contact between tyre and snow surfaces.

4.2 TYRE HYDROPLANING SIMULATIONS

To show the water removal capacity of sipes, tyres with smooth cap, block patterned tread and block patterned tread with sipes as shown in Figure 4.1(a), Figure 4.1(b) and Figure 4.1(c) have been rolled over a 2 cm thick SPH water layer. Water material properties have been taken from SIMULIA/Abaqus Impact of a water-filled bottle example problem (SIMULIA Inc. 2014) and presented in Table 4.1

Water has been modeled using the Equation of state (Eos) option with linear $U_s - U_p$ Hugoniot form. A 170 kPa pressure inflated tyre is loaded on a rigid road with 4000 N load and a SPH water layer is placed on road as shown in Figure 4.2. Water particles are constrained by a rigid box around it.

Table 4.1: Equation of state parameter for water in linear $U_s - U_p$ Hugoniot form

C_0	s	Γ_0
1500	0	0
Density (kg/m^3)	Dynamic viscosity (Ns/m^2)	
996	0.00089	

where, U_s is shock velocity, U_p is particle velocity, Γ_0 is a material constant, C_0 and s define the linear relationship between U_s and U_p (SIMULIA Inc. 2014).

The Linear velocity of tyre is increased from 0 m/s to 28 m/s in x-direction and all other degrees of freedom are constrained except rotation about y-axis, x-direction displacement (to move forward) and z-direction displacement (to load and lift from the road during hydroplaning). The friction coefficient between water and all other components are taken as zero.

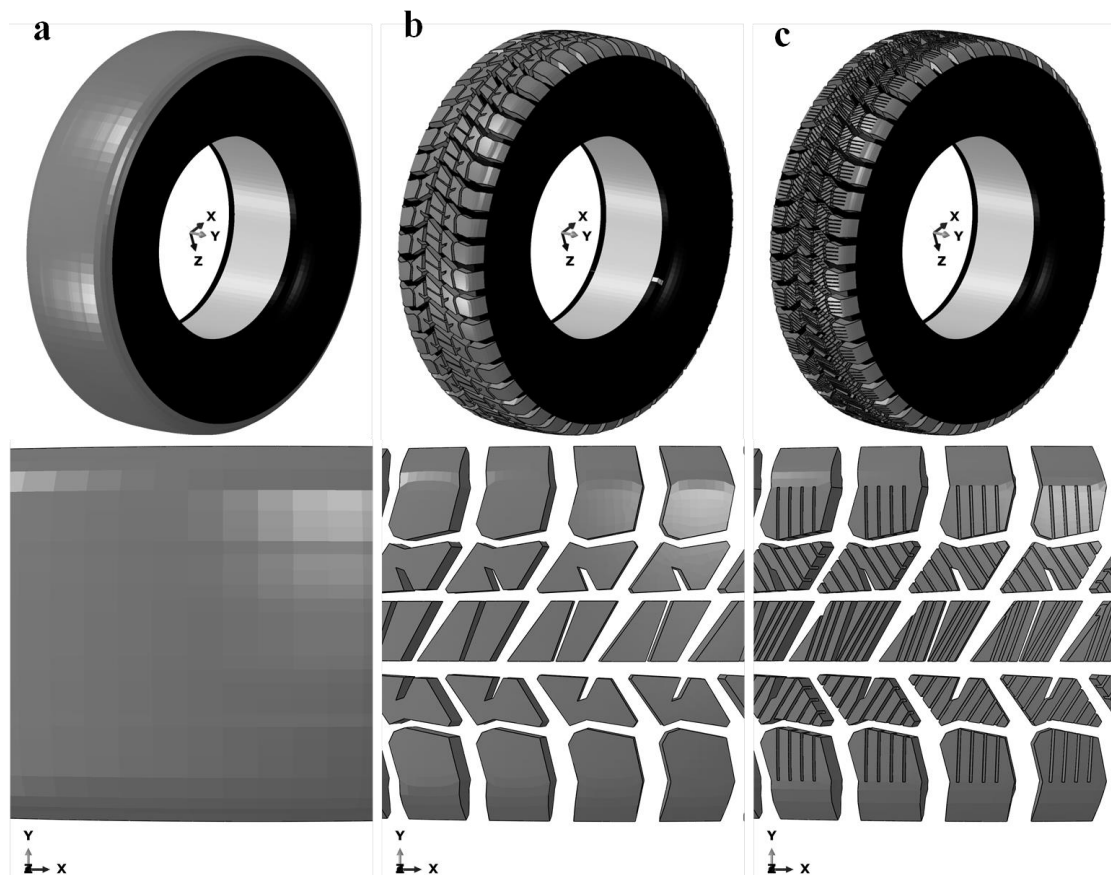


Figure 4.1: Different Tread Geometry of (a) Smooth cap tyre (b) Block patterned tread tyre and (c) Block patterned tread tyre with Sipes

The objective of this substudy is to identify the importance of sipes in water removal capacity at contact region. Figure 4.3(a), Figure 4.3(b) and Figure 4.3(c) indicate that the contact pressure of tyre with sipes is significantly higher than other two tyres. Sipes are the small slits made in the tread to create teeth like prjections. The material removal reduces the available area to support vehicle load on road that leads to the higher contact pressure at contact patch.

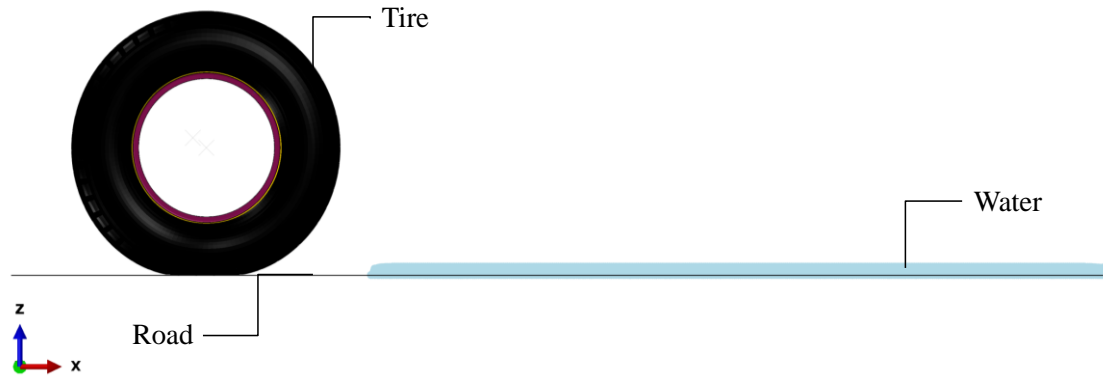


Figure 4.2: Tyre-water assembly for hydroplaning

This higher contact pressure punctures the water and establishes solid to solid contact between tyre and road. Sipes bend, sweep and store the water from contact patch. At critical velocity, tread would not be able to remove water from contact patch and the tyre starts to float on the water without traction. Owing to the above stated reasons, a tyre with sipes operates at higher critical velocities than others as observed in Table 4.2.

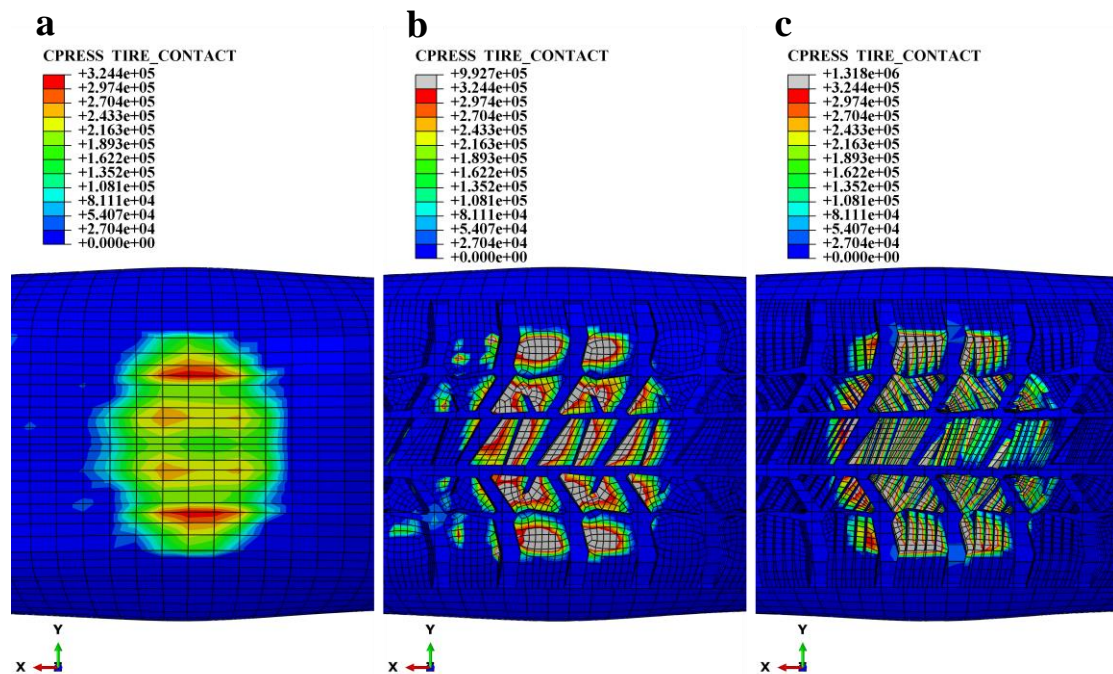


Figure 4.3: Contact pressure of loaded (a) Smooth cap tyre, (b) Block patterned tread tyre and (c) Block patterned tyre with sipes

Table 4.2: Critical velocity of hydroplaning

Tread type	Critical Velocity (m/s)
Smooth cap	11.536
Block patterned tread	14.046
Block patterned tread with sipes	27.250

4.3 FRICTION COEFFICIENT DIFFERENCE BETWEEN BLOCKS WITH AND WITHOUT SIPES

Ella *et al.* (2013) conducted an experiment to find the effect of sipes on coefficient of friction in snow. A rubber block with and without sipes was made to slide over a compacted snow using linear tribometer. The approximate friction coefficients of rubber block without and with sipes in snow are 0.3 and 0.45 respectively. The difference in friction coefficient is due to the water removal capacity of sipes from contact region.

In this work, a numerical procedure is implemented to show the difference in friction coefficient between block with and without sipes.

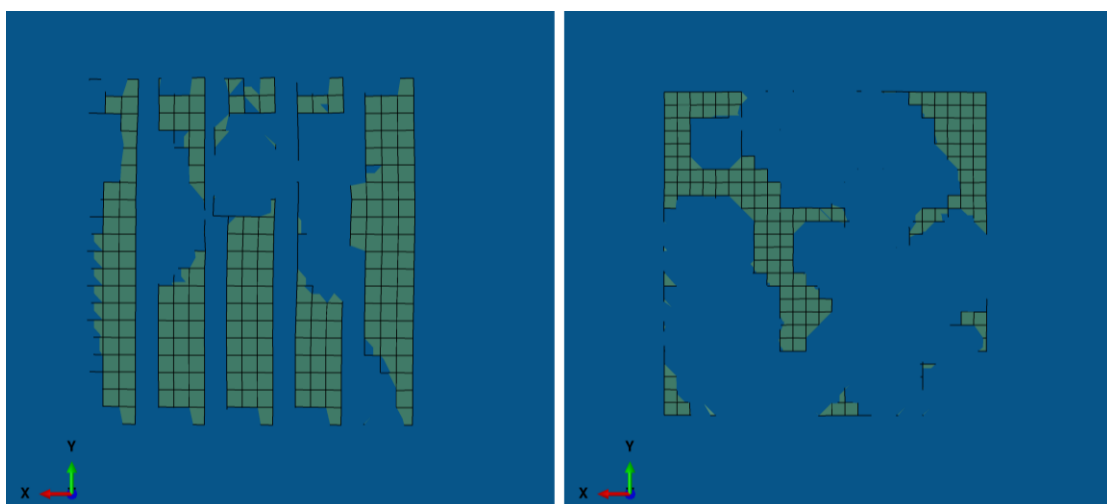


Figure 4.4: Contact area of rubber block with sipes (left) and without sipes (right) on rigid surface with water; Blue regions indicate water

The compacted snow is assumed as a rigid surface and the water due to frictional heat is modeled as SPH water layer. A $0.05 \times 0.05 \times 0.02 \text{ m}^3$ block is used to model blocks with and without sipes. The width of sipe is 1 mm and the depth is 10 mm. The friction coefficient between rubber and rigid surface is taken as 0.3. The friction between water and all other components is taken as zero. Load is applied on the rubber block and a sliding velocity of 0.5 m/s is applied to the top surface of the block using a kinematic coupling.

As expected, Figure 4.4 shows that the rubber block with sipes has more contact area on the rigid surface than rubber block without sipes. This higher area leads to the increase in longitudinal force in rubber block with sipes as observed in Table 4.3. In numerical simulations, three different loads have been applied on rubber blocks and the longitudinal forces (x direction) have been measured. The minimum difference in friction coefficient is approximately 0.15 as seen in Table 4.3. The results obtained from the simulations are close to that obtained by Ella et al. (2013) experimentally.

Table 4.3: Variation of Longitudinal force and Friction coefficient with load

Load (P) (N)	Longitudinal Force (F) (N)		Friction Coefficient (μ) $\mu = (F / P)$		Difference in Friction coefficient
	Without sipes	With sipes	Without sipes	With sipes	
200	4	40	0.020	0.200	0.180
300	25	71	0.083	0.236	0.153
400	27	85	0.067	0.212	0.145

4.4 SUMMARY

These studies prove that the sipes increase the contact area by removing water and that leads to an increase in friction coefficient. Creating the melting snow due to heat energy generated by rolling tyre into the numerical simulation is not the scope of this work. Instead, the temperature effect on melting snow has been brought into the

numerical simulation by means of an equivalent friction coefficient which accounts the water created by the melting of snow and the effect of sipes.

CHAPTER 5

LONGITUDINAL SLIP-FORCE CHARACTERISTICS

5.1 PARTICLE DENSITY STUDY

In order to fix the distance between particles in SPH snow model, plate-sinkage tests have been carried out with different particle distances. SPH with cubic kernel function has been chosen based on previous plate-sinkage test results from Chapter 3.

Table 5.1 shows that a uniform particle density of 10 mm between nodes predicted displacement that are close to that obtained experimentally (Haehnel and Shoop 2004). The densification of snow under compressive load is uniform and realistic for this condition as seen in Figure 5.1(a), Figure 5.1(b) and Figure 5.1(c).

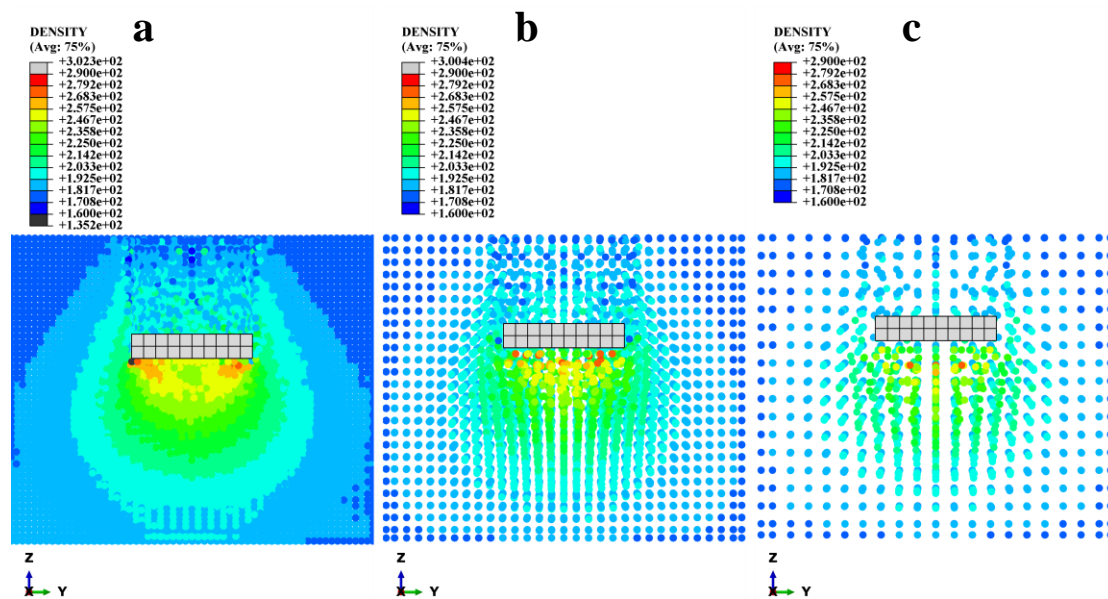


Figure 5.1: Density contours for the cut sections of Plate-Sinkage tests with uniform node density of (a) 0.01 m, (b) 0.02 m and (c) 0.03 m

In subsequent tyre-snow interaction simulations, snow is modeled using SPH with cubic kernel function and with the uniform particle density of 10 mm between particles.

Table 5.1: Plate-Sinkage test comparison with different distance between particles

Distance between Nodes (<i>mm</i>)	Plate Displacement (<i>m</i>)
10	0.198
20	0.180
30	0.168

5.2 SIMULATION PROCEDURE TO OBTAIN LONGITUDINAL SLIP-FORCE CURVE FOR SNOW TYRES

5.2.1 Tyre Axis System

The tyre axis system used in this study is ISO 8855 which has positive upward z-axis as shown in Figure 5.2.

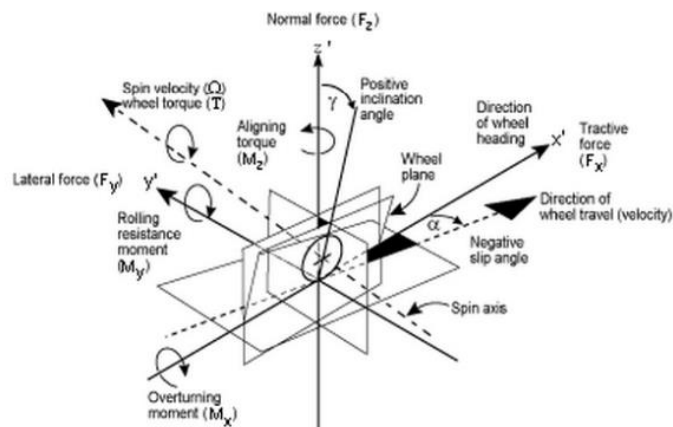


Figure 5.2: Local wheel coordinate as given in ISO 8855

(Source: Fernández 2012)

5.2.2 Finite Element Model of a Pneumatic Tyre

An inflated tyre is symmetric about an axis with respect to geometry and loading condition and a block patterned tread is not symmetric about this axis. Instead of creating a direct three-dimensional (3D) tyre model, firstly, a two-dimensional (2D) axisymmetric tyre model has been modeled without tread pattern as shown in Figure

5.3(a). Different material properties and parameters of reinforcements in tyre are given in Table 5.2 and Table 5.3.

Table 5.2: Elastic properties of different reinforcement

Tyre Components	Density (kg/m^3)	Young's Modulus (N/m^2)	Poisson's Ratio
Bead	7570	206×10^9	0.3
Membrane Ply	1068	4.93×10^9	0.49
Belt 1 and Belt 2	7618	218×10^9	0.3

Table 5.3: REBAR parameter for different reinforcements

Tyre Components	Cross-sectional area (m^2)	Spacing (m)	Orientation (deg)
Ply	3.52257×10^{-7}	9.67740×10^{-4}	2
Belt 1	1.96128×10^{-7}	1.47828×10^{-3}	66.7
Belt 2	1.96128×10^{-7}	1.47828×10^{-3}	-66.7

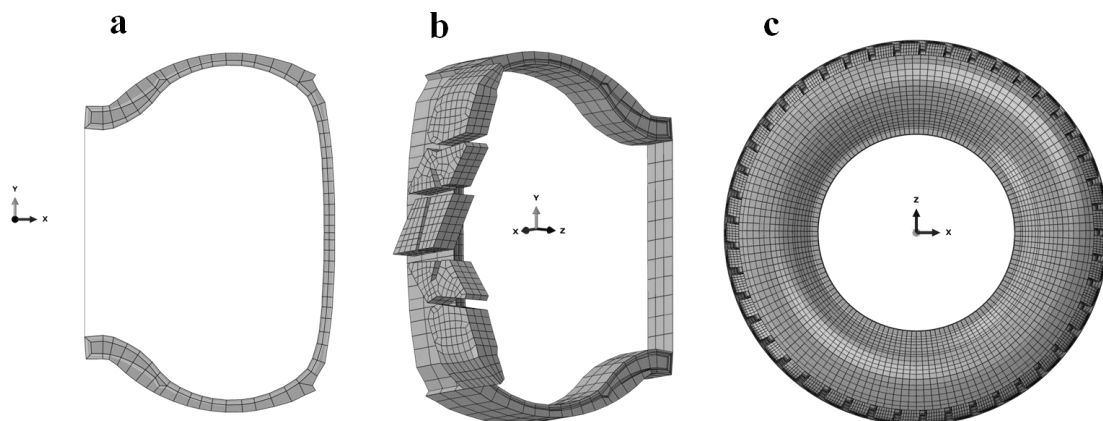


Figure 5.3: FE model of tyre. (a) Inflated two-dimensional (2D) axisymmetric tyre model without tread (b) Adding a tread section to the three-dimensional (3D) tyre section model (c) Full 3D tyre model

In this study, the rubber components are modeled using reduced polynomial with strain energy potential of order 3 material model (SIMULIA Inc. 2014) and the parameters are presented in Table 5.4.

Table 5.4: Reduced polynomial model parameter for different rubber region

Tyre Components	Density (kg/m^3)	C₁₀ (N/m^2)	C₂₀ (N/m^2)	C₃₀ (N/m^2)
Belt 1	1198	1024720	- 427524	173328
Belt 2	1198	1024720	- 427524	173328
Filler	1204	1042180	- 391161	134412
Inner liner	1177	479895	- 135723	43677
Ply	1177	479895	- 135723	43677
Rim strip	1153	666402	- 208725	65205
Sidewall	1118	473685	-119853	34293
Tread	1178	777561	- 276138	95427

A repetitive section of a block patterned tread has been added to the circumferential section of the tyre to create a pitch model as shown in Figure 5.3(b). An inflated full 3D tyre model has been created by using ABAQUS symmetric model generation from a pitch (of the tyre) model as seen in Figure 5.3(c). But in smooth cap tyre model, the tread is also symmetric about axis, so that the pitch file generation is not needed to create a full 3D tyre model.

5.2.3 Procedure to Obtain Longitudinal slip-Force Characteristics

To obtain longitudinal slip-force curve, a series of analyses is needed. The loading of the tyre on snow for each analysis is computationally demanding. To avoid this, the tyre is loaded on road and rolled with a prescribed linear velocity by using ABAQUS/Explicit as shown in Figure 5.4(a) with all other degrees of freedom are

constrained except rotation about y-axis, x-direction displacement (to move forward) and z-direction displacement (to load). These conditions are continued in snow by applying a particular angular velocity for a particular slip ratio by using ABAQUS Import option. At zero torque, the RRM created due to tyre sinking depth acts as a braking torque which produces RRF or braking force. To find RRM, tyre is towed (no torque applied) in snow with a particular linear velocity and from ABAQUS history output, Reaction Moment 2 (RM2) is measured at rim node. In this study, the zero slip condition is defined to be that condition under which the tyre rolls in snow with zero traction force. To obtain zero slip condition, the value of RM2 is applied as torque at rim node to equate RRM in order to get zero traction force as shown in Figure 5.4(b). The longitudinal slip (σ) is defined as,

$$\sigma = -\left(\frac{v_x - r\omega}{r\omega}\right) \quad (5.1)$$

Where v_x is linear velocity, ω is angular velocity and r is zero slip radius of tyre.

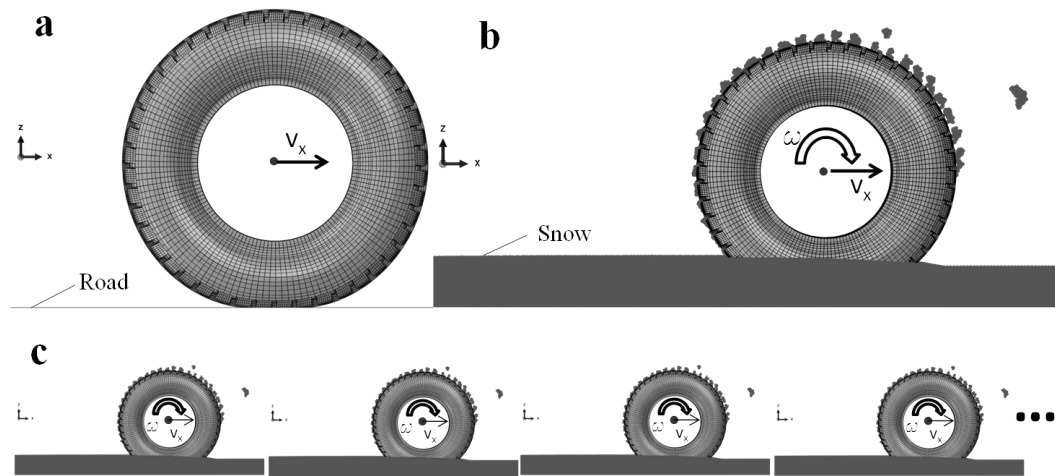


Figure 5.4: Procedure to obtain longitudinal slip-force curve. (a) Loading and rolling the tyre on road (b) Rolling the tyre in snow to find zero slip condition (c) Series of analyses to find forces in each slip ratio

The value of r can be calculated by measuring the length (L) travelled by the tyre for one revolution in snow, under zero traction. This length is the circumference of the rolling tyre and $r = \frac{L}{2\pi}$. The angular velocity at zero slip condition is calculated by dividing linear velocity by zero slip radius of tyre. In Equation (5.1) by fixing σ , r and v_x the angular velocity for a particular slip ratio can be calculated. Series of analyses

has been conducted to obtain longitudinal slip-force curve by fixing linear and angular velocities in each analysis as seen in Figure 5.4(c).

In this study, a 170 kPa pressure inflated smooth cap tyre is loaded in a $3.5 \times 0.6 \times 0.12 \text{ m}^3$ SPH soft snow terrain with 4000 N load and 2.7778 m/s linear velocity has been applied at rim node. The material properties of soft snow are presented in Table 3.1. The RRM in towing condition at rim node is 45 Nm and the corresponding zero slip radius is 0.42 m. By using Equation (5.1), angular velocities are calculated for corresponding slip ratios from which, longitudinal slip-force curve obtained.

5.3 IS LONGITUDINAL SLIP-FORCE CURVE SUITABLE FOR SNOW TYRES?

In tyre-road interaction analysis, the zero slip radius is a function of load, inflation pressure and linear velocity (Pacejka, 2006). These quantities are invariant in all slip ratios and nothing is ahead of the rolling tyre to resist motion. The variation in vertical displacement of rim node (z-direction as shown in Figure 5.4) is minimal for all slip ratios as shown Figure 5.5.

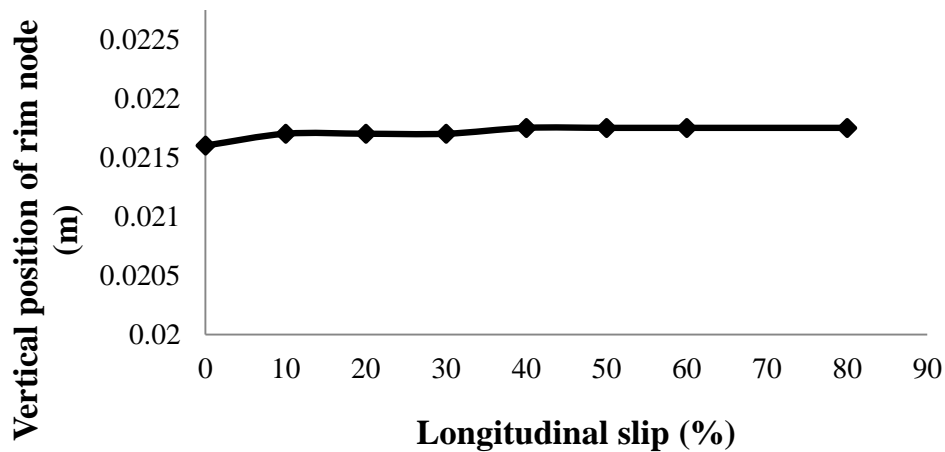


Figure 5.5: Variation of vertical position of rim node on road

Hence the zero slip radius of tyre can be taken as the reference value for all slip ratios. However in tyre-snow interaction analysis, the snow resists the linear and angular motion of tyre due to tyre sinking. Unlike the road, these resistances are a function of tyre sinking depth into the snow and the cohesion stress value of snow. Based on the procedure explained for snow tyres, the zero slip radius is calculated. In order to compare the results with road, a graph similar to Figure 5.5 is drawn for snow (Figure 5.6).

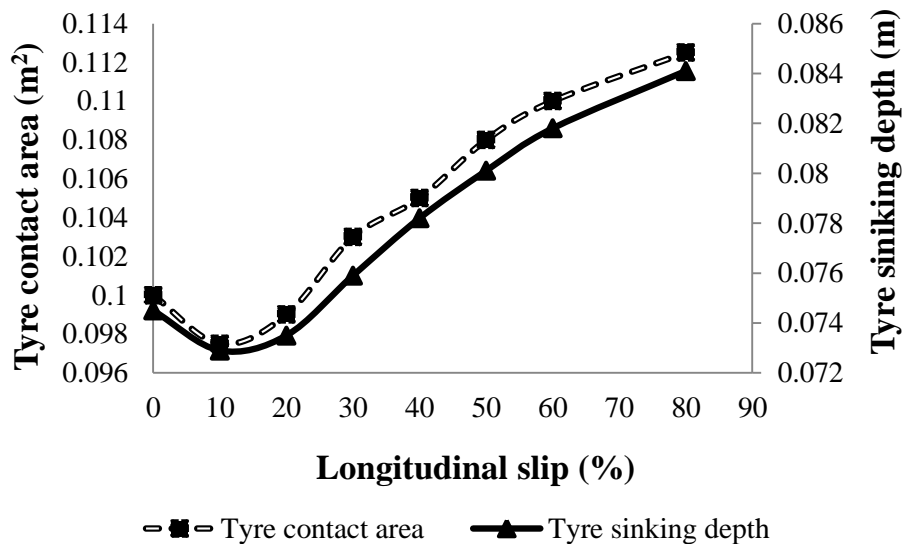


Figure 5.6: Variation of tyre sinking depth and tyre contact area in snow

In Figure 5.6, up to 10 % slip ratio, the tyre sinking depth decreased and after that it increased. This decrease and increase in tyre sinking depth is due to the climbing and digging action of the tyre with an increase in angular velocity. Due to this, in Figure 5.7, the motion resistance force due to snow ahead of rolling tyre, marginally decreases and increases at higher slip ratios. In smooth cap tyre, the force due to compressed snow is absent and the net longitudinal force due to contact pressure is equal to the motion resistance force. On the other hand for a patterned tyre, the net longitudinal force due to contact pressure is the algebraic sum of force due to the compressed snow in grooves and the motion resistance force. The tyre contact area increases with increase in tyre sinking depth as seen in Figure 5.6. The variation in sinking depth and contact area of the tyre change the resistance to linear and angular motion of the tyre respectively in each slip ratios. The zero slip condition is defined for a particular tyre sinking depth. However the continuous variation in tyre external environment with respect to slip ratio raises the question of using zero slip condition as the reference value for snow tyres.

The drawbar pull is the algebraic sum of traction, which aids motion and motion resistance, which opposes motion. In other words, it is the force required to overcome resistance and a positive drawbar pull indicates the availability of longitudinal force for acceleration. Up to 65% slip ratio, the draw bar pull is negative as observed in Figure 5.7. The negative drawbar pull can be explained with a simple frictional force analogy as shown in Figure 5.8. In the case of friction, when the applied force (P) is less than the frictional force (F), the block would not move and the produced

frictional force is equal to the applied force. However, when the applied force reaches the maximum frictional force (μN), the block would start to move. Similarly, the negative drawbar pull indicates that the resistance to motion (similar to μN) is needed to overcome to accelerate the vehicle. In Figure 5.7, region 1 represents the towing phase (driven state) and region 2 represents acceleration phase (driving state). Thus, the vehicle accelerates, if only the drawbar pull is zero or positive. From Figure 5.7, the drawbar pull reaches zero at 65% slip ratio and the maximum force is reached at 80 % slip ratio. This is not what is usually observed in tyre mechanics.

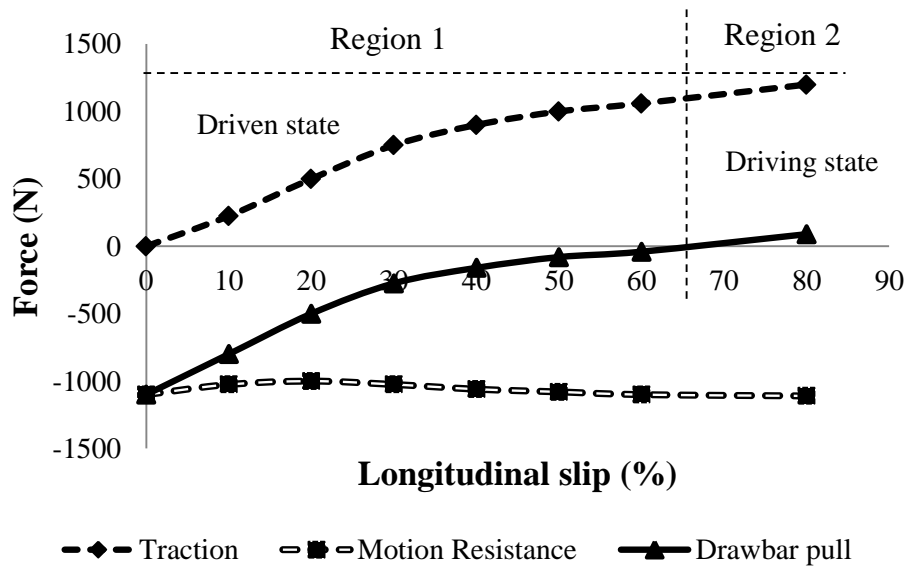


Figure 5.7: Variation of Traction, Motion Resistance and Drawbar pull

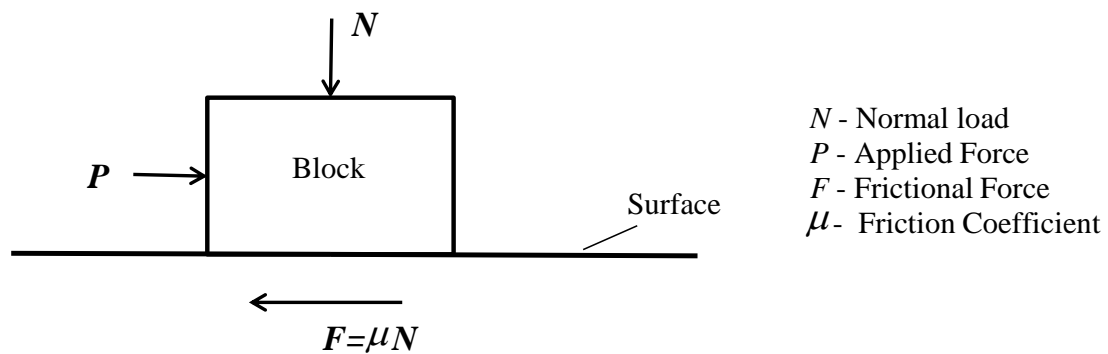


Figure 5.8: Frictional mechanism of a block over a surface

5.4 SUMMARY

Based on the observations from Figure 5.6 and Figure 5.7, resistance to linear and angular motion of the tyre increases with respect to slip ratio, due to an increase in tyre sinking depth. Owing to the continuous variation in the tyre external environment, zero slip radius also varies with respect to slip ratio. Hence, the longitudinal slip-force characteristics for uncompacted snow is not similar to a tyre on road and cannot be interpreted in the same fashion. However, a compacted snow terrain behaves like a road and the longitudinal slip-force characteristics might be suitable for such conditions.

In order to provide a physical understanding of tyre-snow interaction, the forces are plotted with respect to torque. The torque-force characteristics are similar to longitudinal slip-force characteristics as observed from Figure 5.9 and Figure 5.7. But, torque is a constant input parameter which is independent of tyre sinking depth. The procedure to obtain torque-force characteristics and its physical understandings are explained in Chapter 6.

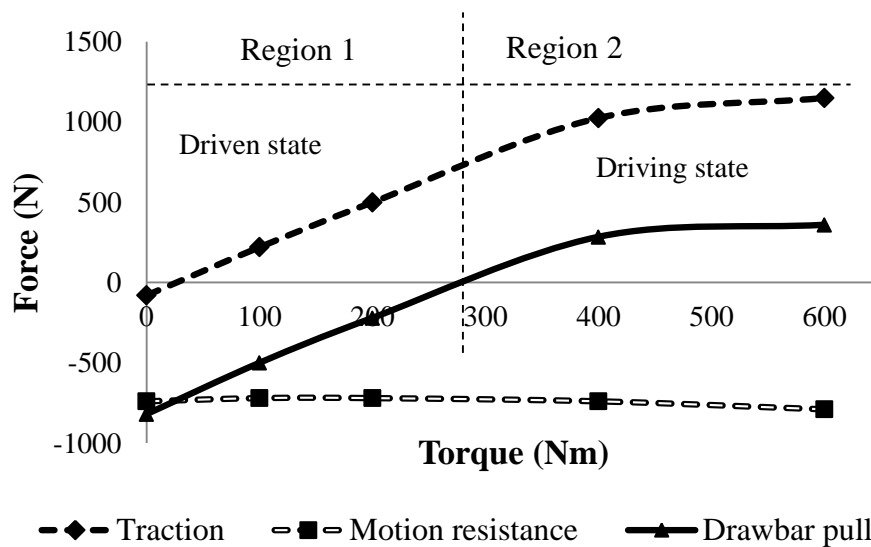


Figure 5.9: variation of Traction, Motion resistance and Drawbar pull with respect to torque for a smooth cap tyre

CHAPTER 6

TORQUE-FORCE CHARACTERISTICS

6.1 FINITE ELEMENT MODELING AND PROCEDURE

Based on the observations from Chapter 5, the longitudinal slip-force characteristics is not suitable for snow tyres in uncompact snow terrain. To capture and compare the tyre performance in uncompact snow terrain, a constant input parameter is needed with respect to the depth of sinking and contact area of the tyre. Hence, torque has been taken as the input parameter for all analyses. The procedure used to obtain torque-force characteristics is explained in Figure 6.1. The 3D tyre has been modeled using 2D axisymmetric model and pitch model (shown in Figure 6.1(c), Figure 6.1(a) and Figure 6.1(b)). A series of analyses are needed to obtain the force characteristics under different torque values (T) as seen in Figure 6.1(d).

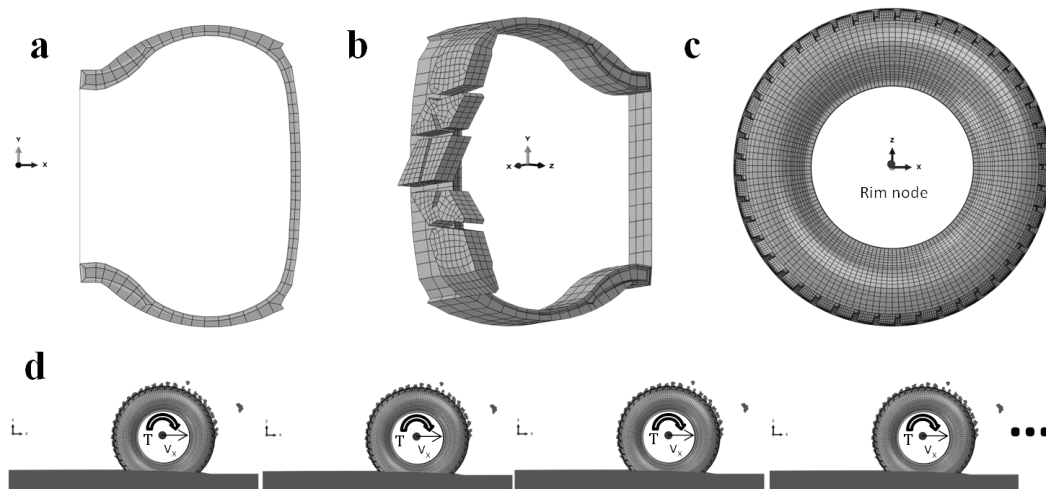


Figure 6.1: Procedure to obtain torque-force characteristics. (a) Inflated two-dimensional (2D) axisymmetric tyre model without tread (b) Adding a tread section to the three-dimensional (3D) tyre section model (c) Full 3D tyre model (d) Series of analyses to find forces under different torque

The procedure to obtain torque-force characteristics is similar to that of longitudinal slip-force characteristics. Here, the torque has been applied at the rim node instead of an angular velocity. Smooth cap, block patterned tread and block patterned tread with sipes tyres are inflated to 200 kPa pressure and loaded with 4000 N load. As explained in the in Chapter 4, instead of modeling sipes in tyres, an equivalent friction

coefficient can be assigned between sipes surface and snow. In this study, the block patterned tread tyre with sipes is represented using a block patterned tread tyre with an equivalent friction coefficient of 0.45 between tread top surface and snow, while other contact surfaces are assigned with a 0.3 friction coefficient. In smooth cap tyre and block patterned tread tyre analyses, a friction coefficient of 0.3 is assigned between tyre contact and snow. A SPH snow block of $2.9 \times 0.6 \times 0.09 \text{ m}^3$ is used for all torque-force analyses.

All the results have been taken at the steady state region and before the end of one revolution of the tyre, to remove the effect of sticking snow in the tyre grooves on the contact forces. Figure 6.2 showed that the tyre completed one revolution in 0.38 seconds for 600 Nm torque and 0.28 seconds for 800 Nm torque. At 800 Nm torque, the tyre completed one revolution before it reaches the steady state. This 0.1 second difference is the limiting criteria for the tyre used in this study to extract results. Hence in this study, the torque-force characteristics are restricted to 600 Nm torque.

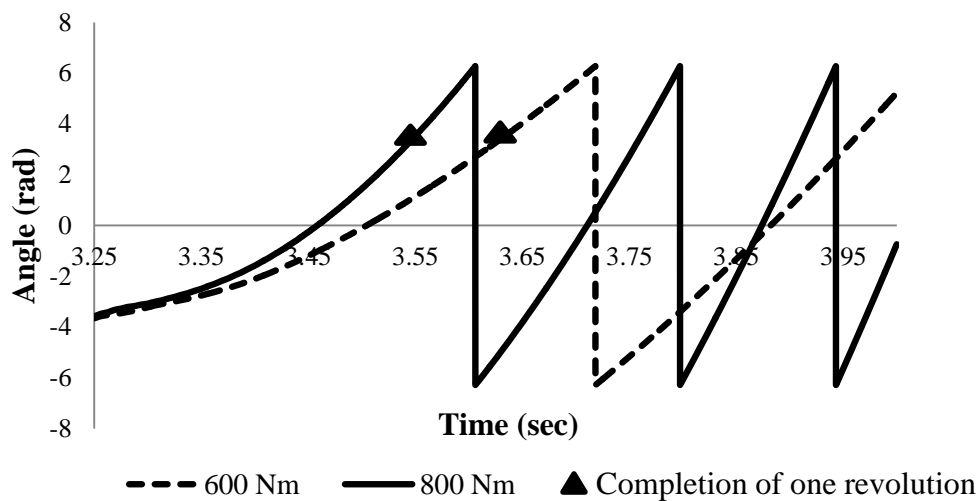


Figure 6.2: Rotational displacement of rim node

6.2 FORCE CHARACTERISTICS OF SMOOTH CAP, BLOCK PATTERNED AND BLOCK PATTERNED TREAD WITH SIPES TYRES IN SOFT SNOW

Soft snow material properties are presented in Table 3.1. In Figure 6.3, the tyre sinking depth variation with respect to torque is observed, which is similar to the variation of tyre sinking depth with respect to longitudinal slip in soft snow. However, unlike the longitudinal slip, the torque is a constant input parameter which is

independent of tyre sinking depth. The tyre sinking depth of block patterned tread tyre is higher than the smooth cap tyre due to the digging action of tread blocks as seen in Figure 6.3 and this increases the RRM in block patterned tread tyre.

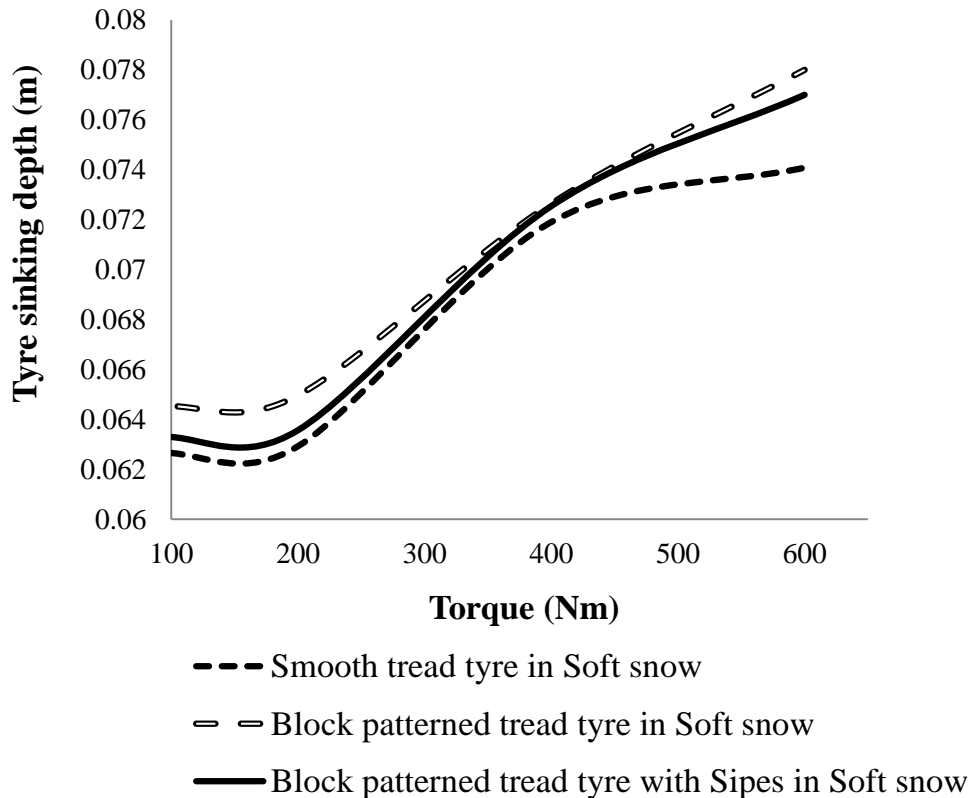


Figure 6.3: Variation of tyre sinking depth in soft snow

In sum, there are four forces that act on the tyre with tread:

- Traction Force due to the application of torque. The fundamental mechanism is tread deformation. This aids motion of the wheel.
- Rolling Resistance Force (RRF) due to rolling resistance moment
- Gear effect due to tread block. The presence of snow between the treads helps in propulsion. This is analogous to an increase in friction and can act with no slip as well.
- Opposing force, consisting of two forces, namely, motion resistance force due to a heap of snow lying ahead of the tyre and the shear strength of snow between the tread.

Figure 6.4 represents the algebraic sum of traction force and RRF. In Figure 6.4, the initial negative values of forces are representing the RRF, which is the amount of force that is needed to be applied through torque at the axle to overcome the

RRM. The increase in torque overcomes the RRM and increases the traction force. The compressed snow in grooves of tread pattern resists the tread deformation but in smooth cap tyre, the cap region is free to deform. Due to this, the smooth cap tyre has higher traction force than other two tyres and the block patterned tread tyre with sipes has higher traction force than block patterned tyre, because of the increase in friction coefficient as seen in Figure 6.4. The less deformation of block patterned tread compared to smooth cap, enables the block patterned tread tyre to work at higher slip range than smooth cap tyre.

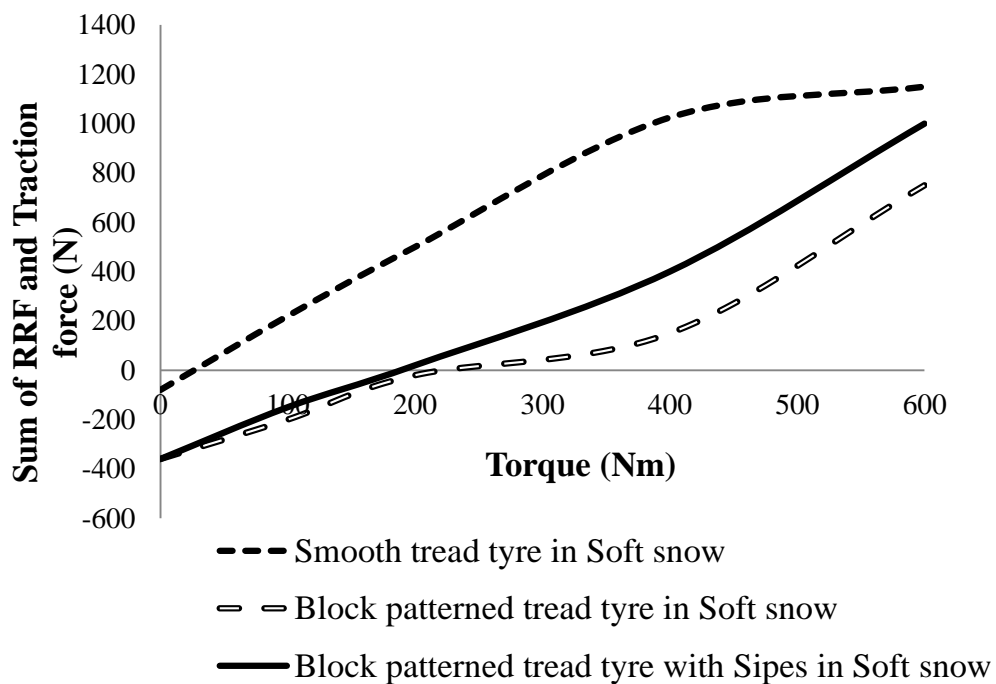


Figure 6.4: Variation of traction force in soft snow

The net longitudinal force due contact pressure is the algebraic sum of motion resistance force and force due to compressed snow in grooves. At zero torque, the motion resistance force dominates the force due to compressed snow in grooves in both block patterned tread tyre and block patterned tyre with sipes as seen in Figure 6.5. However, when the torque value increases, the force due to compressed snow dominates the motion resistance as observed in Figure 6.5.

In smooth cap tyre, force due to compressed snow in grooves is absent and motion resistance varies with respect to tyre sinking depth. From Figure 6.5 and Figure 6.3, though the tyre geometry is same for both block patterned tread tyre and tyre with

sipes, the difference in the force and tyre sinking depth is due to the change in friction coefficient between them.

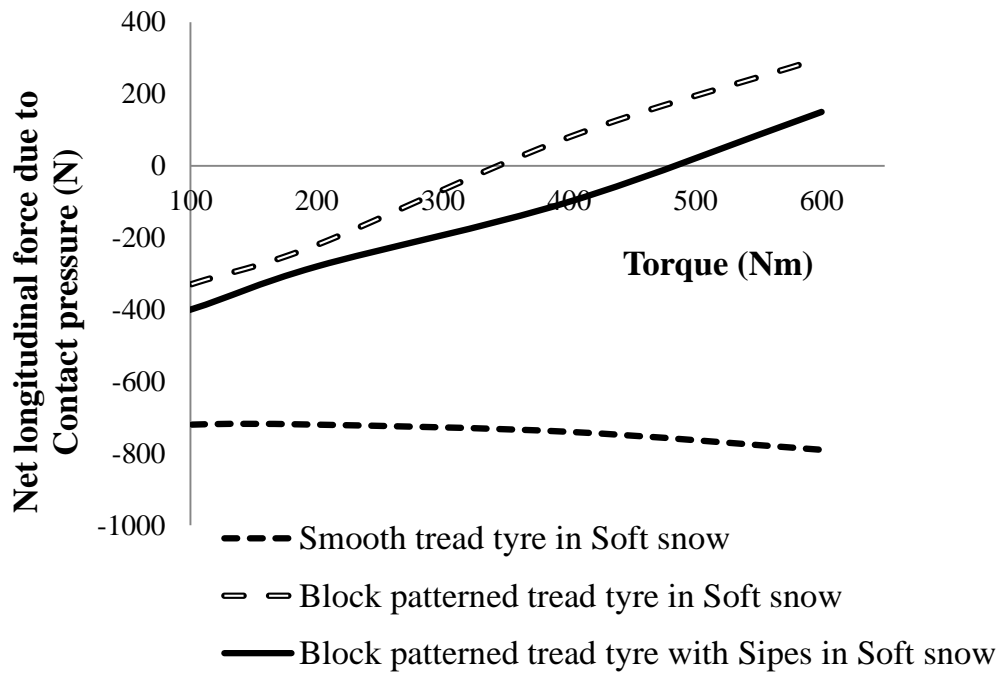


Figure 6.5: Variation of net longitudinal force due to contact pressure in soft snow

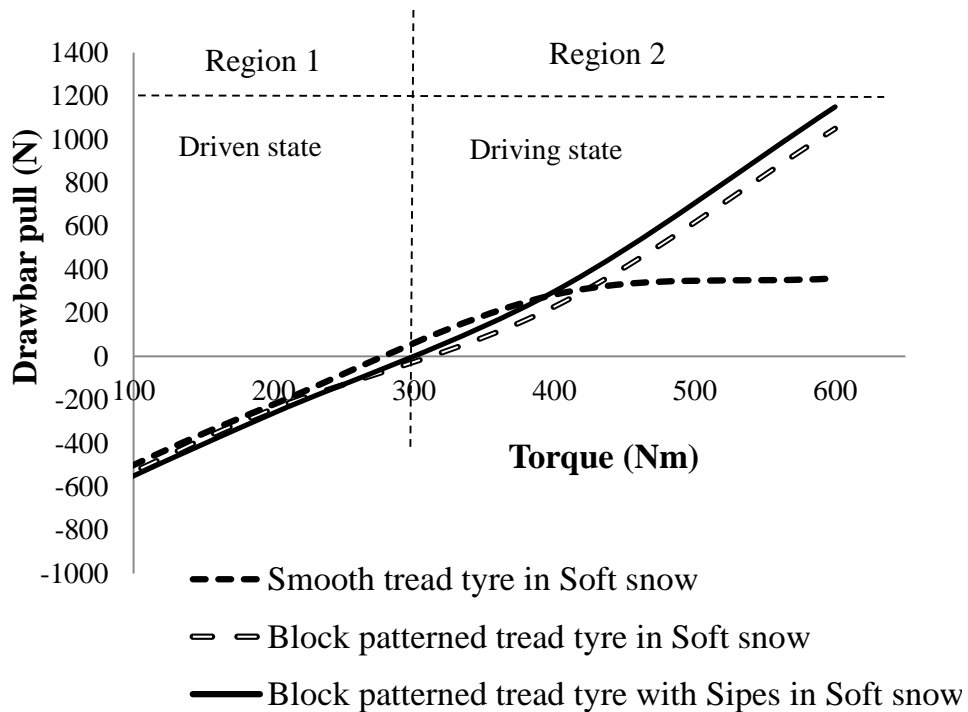


Figure 6.6: Variation of drawbar pull in soft snow

The drawbar pull is algebraic sum of RRF, traction force and net longitudinal force due to contact pressure. In sum, though the smooth cap tyre has higher traction force

for a particular torque, the net available longitudinal force due to contact pressure is less due to the absence of force due to compressed snow in grooves. The block patterned tread tyre with sipes shows higher drawbar pull in region 2 (Driving state) due to the increase in net longitudinal force due to contact pressure with respect to torque and higher friction coefficient as shown in Figure 6.6.

6.3 FORCE CHARACTERISTICS OF SMOOTH CAP, BLOCK PATTERNED AND BLOCK PATTERNED TREAD WITH SIPES TYRES IN HARD SNOW

The identical tyres, snow dimensions, particle density and boundary conditions have been used to obtain the torque-force characteristics of tyres in hard snow. To model hard snow, the cohesion stress and the cap eccentricity values have been taken as 30000 N/m^2 and 0.00011 respectively from the literature (Shoop 2001). The tyre behaviour in hard snow is similar to the behaviour in soft snow as seen in Figure 6.7, Figure 6.8, Figure 6.9 and Figure 6.10.

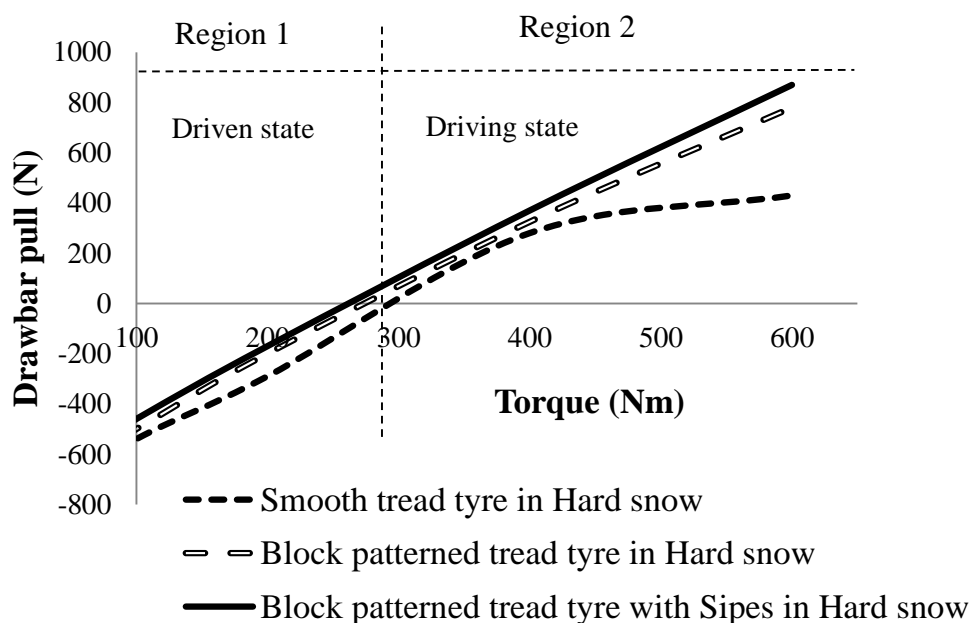


Figure 6.7: Variation of drawbar pull in hard snow

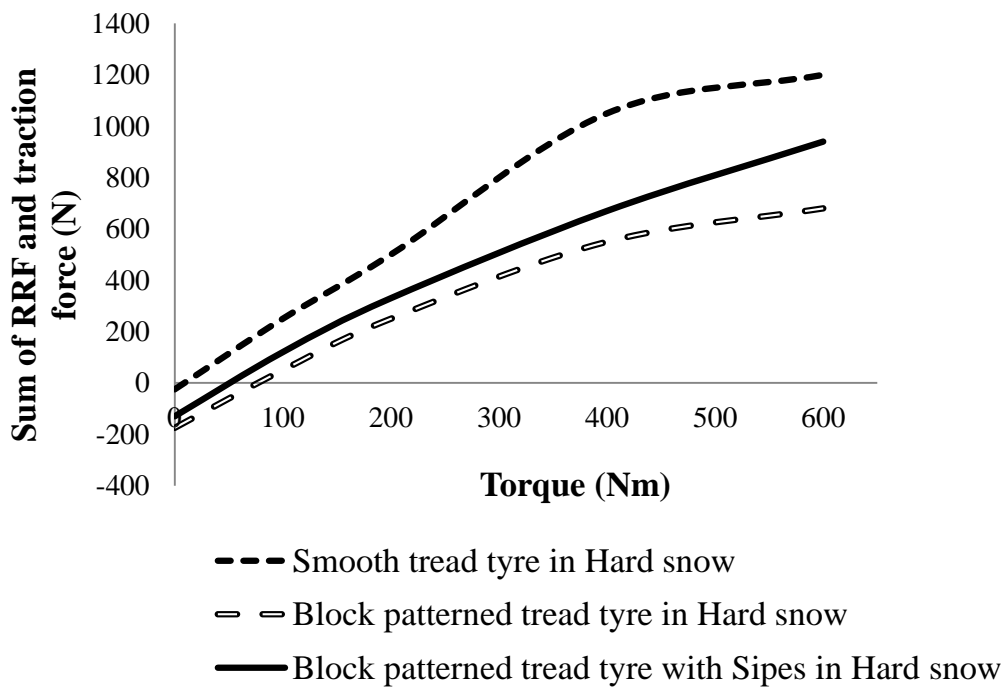


Figure 6.8: Variation of traction force in hard snow

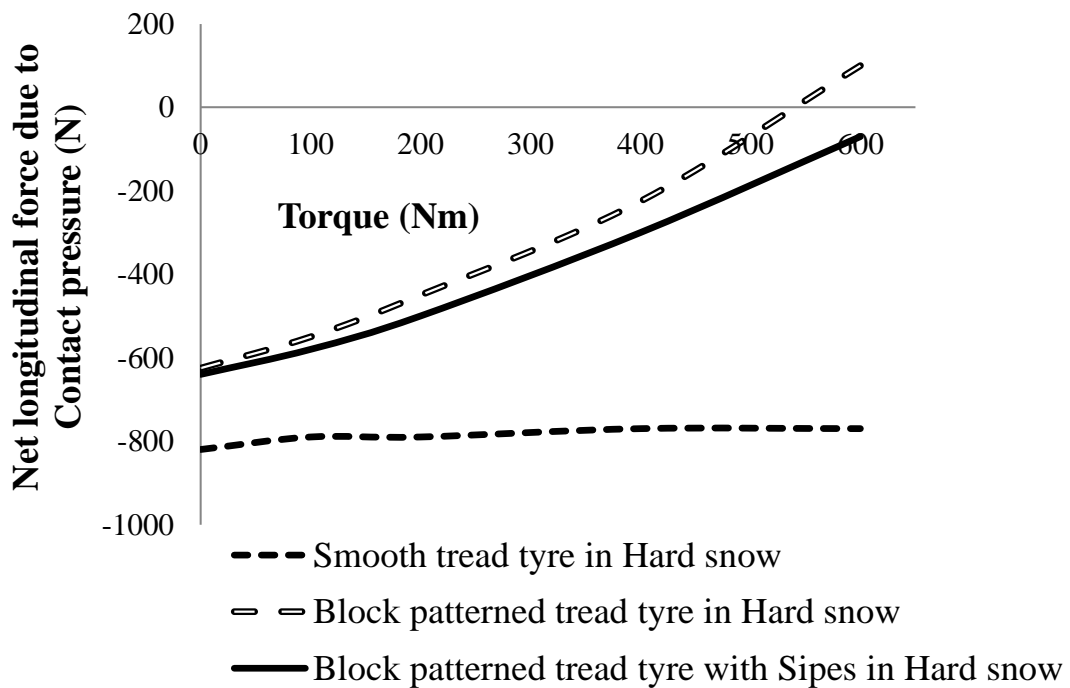


Figure 6.9: Variation of net longitudinal force due to contact pressure in hard snow

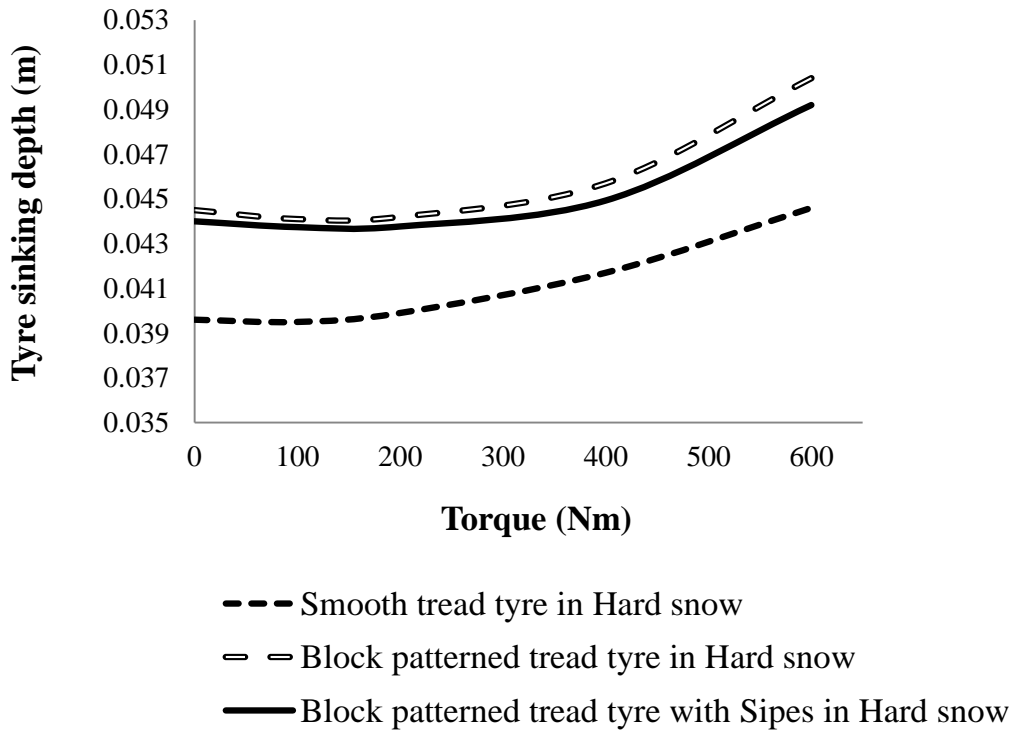


Figure 6.10: Variation of tyre sinking depth in hard snow

6.4 COMPARISON OF TYRE PERFORMANCE IN SOFT AND HARD SNOW

Though the tyre behavior is similar in soft and hard snow, the performance characteristics of the tyres are different. The tyre sinking depth in hard snow is less than that in the soft snow due to higher cohesion value as seen in Figure 6.3 and Figure 6.10. Because of this, the RRM is higher for tyres in soft snow and this leads to higher RRF in soft snow as shown in Figure 6.4 and Figure 6.8. In addition to that, for block patterned tread tyres, the shear failure at tread grooves affects the tread deformation.

For 200 Nm torque, the compressed hard snow in grooves is not failed in shear and the compressed soft snow is failed in shear and filled the grooves as seen in Figure 6.11. As the result of this process, the tread deformation is restricted by the filled snow in grooves and reduced the traction force as shown in Figure 6.4 and Figure 6.8.

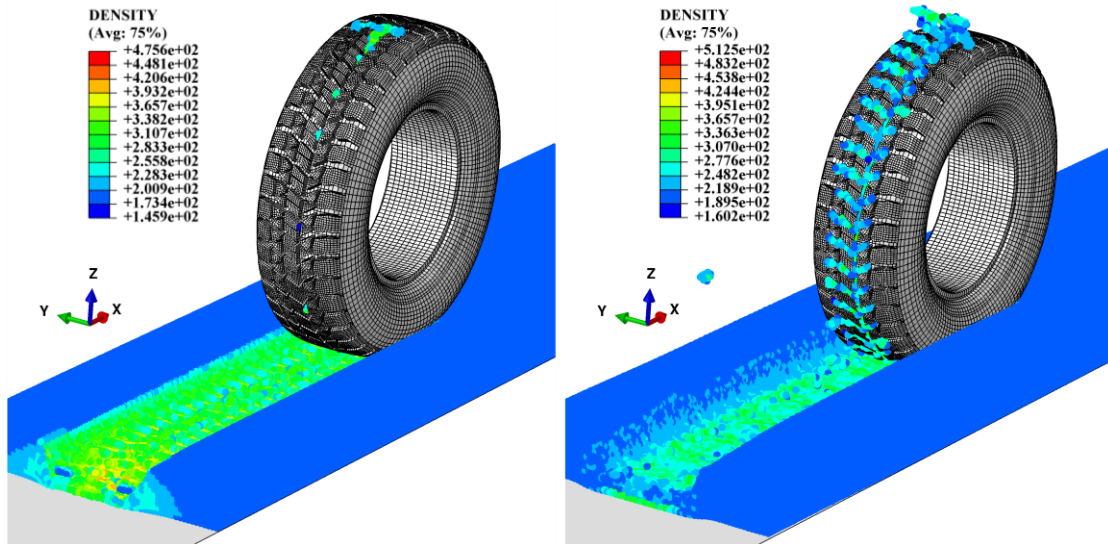


Figure 6.11: Failure of compressed hard snow (left) and soft snow (right) in tread grooves with 200 Nm torque

However for 600 Nm torque, both hard and soft snow are failed in shear at grooves as shown in Figure 6.12. The large cohesion value of hard snow allow the tread to deform less than that in soft snow. Due to this in Figure 6.4 and Figure 6.8, at 600 Nm torque, the traction of block patterned tread tyres in soft snow is greater than hard snow. For smooth cap tyres, the traction performance is approximately same due to free tread deformation.

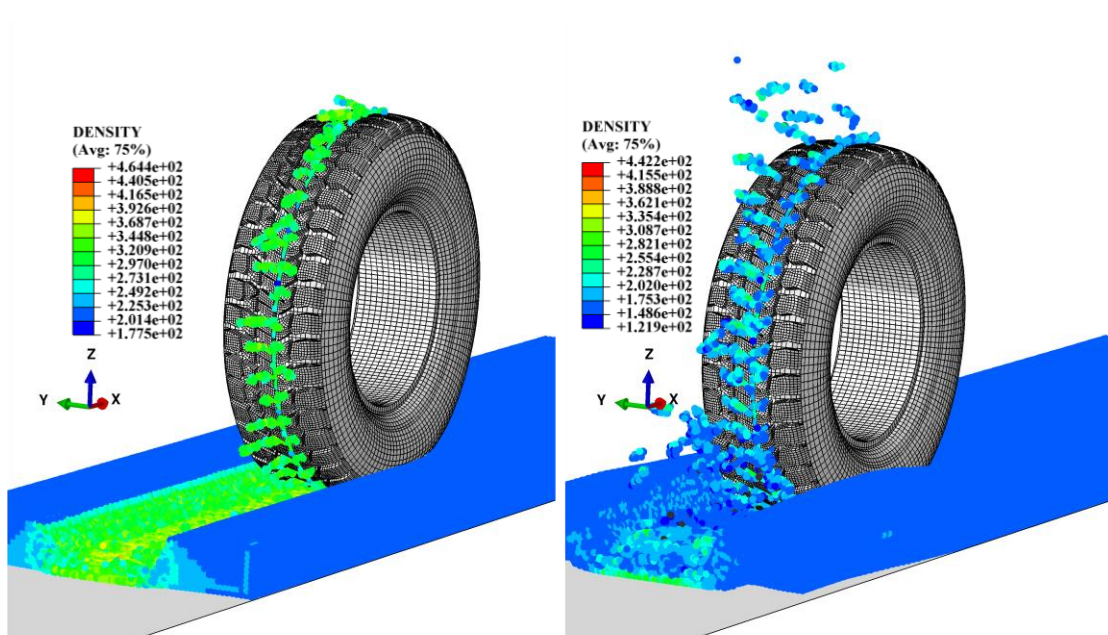


Figure 6.12: Failure of compressed hard snow (left) and soft snow (right) in tread grooves with 600 Nm torque

Net longitudinal force due to tyre contact pressure for a tread patterned tyre is a function of cohesion, tyre sinking depth and shear strength of compressed snow, but for a smooth cap tyre, it is only a function of tyre sinking depth and cohesion. Figure 6.3, Figure 6.10, Figure 6.5 and Figure 6.9 indicate that, though the tyre sinking depth is larger in soft snow, the resistance offered by the cohesion stress of hard snow dominates the motion resistance force. Thus, the net longitudinal force due to contact pressure is higher in soft snow as seen in Figure 6.5 and Figure 6.9. Hence, the drawbar pull of tyres in soft snow for acceleration are higher due to the domination of net longitudinal forces due to contact pressure as observed in Figure 6.6 and Figure 6.7.

6.5 COMPARISON OF TYRE PERFORMANCE WITH DIFFERENT LOADS

The effects of soft and hard snow have been discussed in previous section. Hence for the load comparison, block patterned tread tyre with sipes in hard snow have been used. For comparison, a 6000 N loaded tyre and a 4000 N loaded tyres have been used.

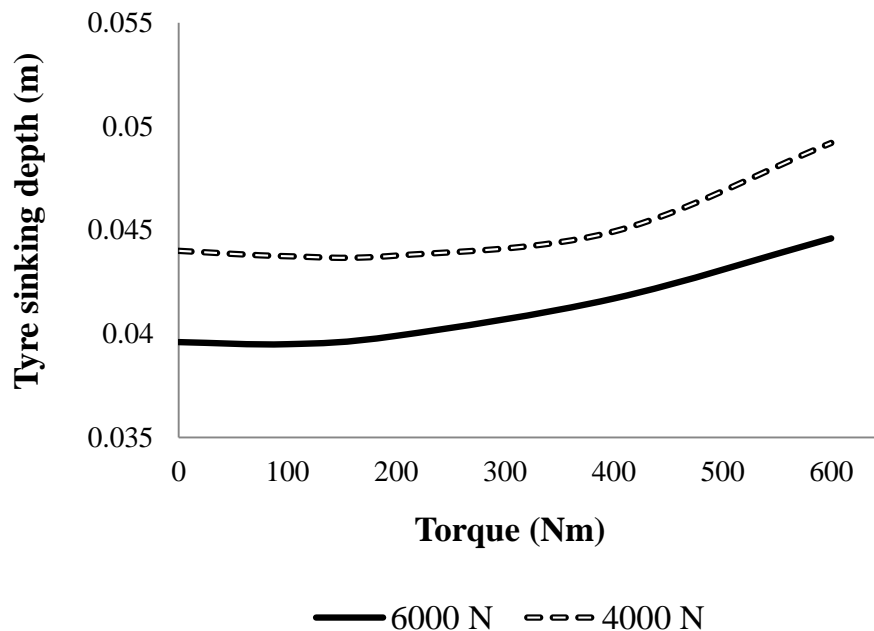


Figure 6.13: Variation of vertical position of rim node with different loads

Figure 6.13 shows that the tyre sinking depth is higher in 6000 N loaded tyre. Due to the higher tyre sinking depth, at zero torque, the RRF is more in tyre loaded with 6000 N load as seen in Figure 6.14. The net longitudinal force due to contact pressure is more in 4000 N loaded tyre as seen in Figure 6.15, due to the less resistance offered

by the volume of snow ahead of rolling tyre. Hence, the tyre loaded with fewer loads has higher traction force and higher net longitudinal force due to contact pressure, because of less tyre sinking depth. Thus the drawbar pull for acceleration is higher in tyre loaded with 4000 N load as shown in Figure 6.16.

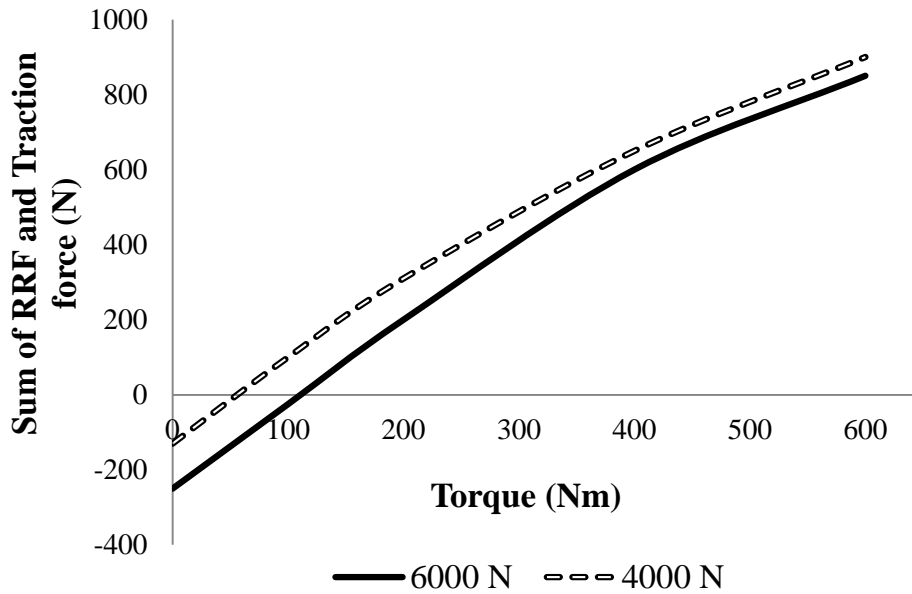


Figure 6.14: Variation of traction force with different loads

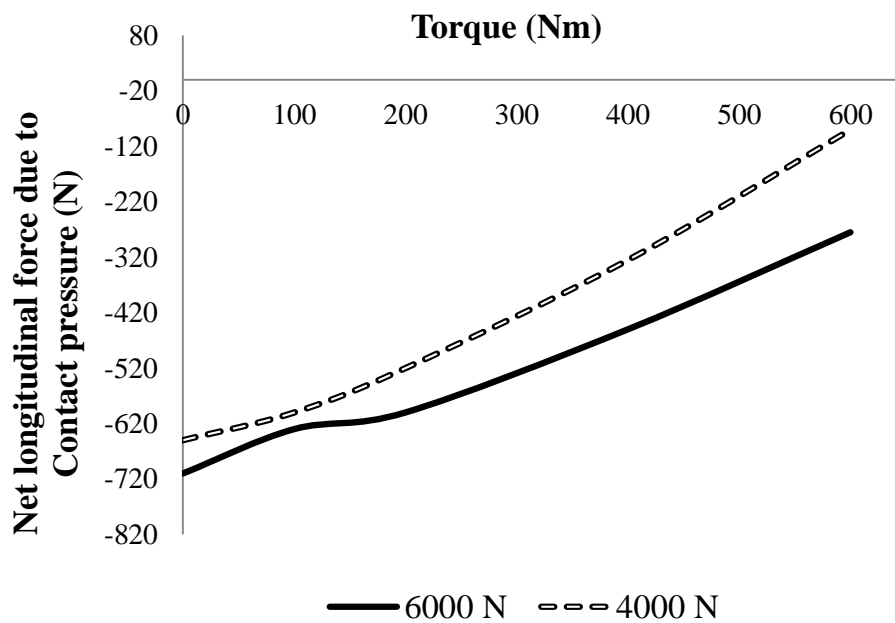


Figure 6.15: Variation of net longitudinal force due to contact pressure with different loads

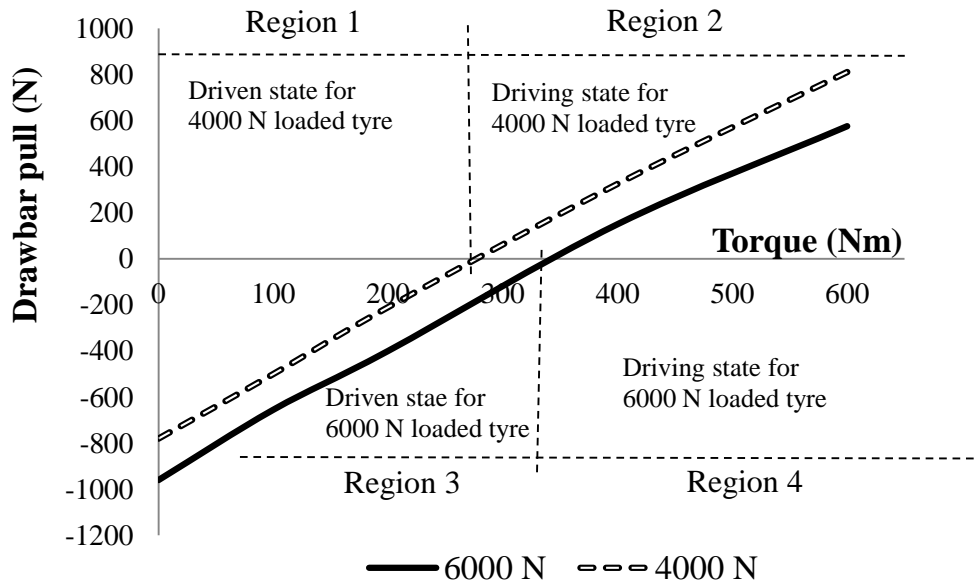


Figure 6.16: Variation of drawbar pull with different loads

Logically, the higher depth snow and higher inflation pressure tyre would have higher tyre sinking depth and behave like 6000 N loaded tyre as seen in Figure 6.13, Figure 6.14, Figure 6.15 and Figure 6.16.

6.6 COMPUTATIONAL TIME

6.6.1 Comparison of the Computational Time of Lagrangian, CEL and SPH Methods

To compare the computational time between Lagrangian, CEL and SPH methods, the plate-sinkage tests, computational times have been taken. Snow is modeled using the uniform node density of 10 mm between nodes in each numerical method with the identical simulation time.

Table 6.1: Computational time comparison of Lagrangian, CEL and SPH methods

Numerical Method	Simulation Time (<i>min</i>)
Lagrangian	102
CEL	154
SPH	431

From Table 6.1, the ratio of the computational time of Lagrangian, CEL and SPH method is $1:1\frac{1}{2}:4\frac{11}{50}$ respectively. Thus the SPH method is a computationally demanding numerical method than other two.

6.6.2 Computational Time to Obtain Torque-Force Characteristics

To obtain the torque-force characteristics for smooth cap tyre, block patterned tread tyre and block patterned tread tyre with sipes in soft snow and hard snow and also for load variation, a total of 40 coupled FEM-SPH analyses have been made. Each analysis has taken around 30 hours of simulation run time in a 12 core computer. Thus a total of 1200 hours have been spent to obtain torque-force characteristics.

CHAPTER 7

CONCLUSION

7.1 CONCLUSIONS

Based on the understanding from this current work, the following conclusions can be drawn:

- A detailed explanation of the mechanism of tyre traction in snow has been given. In the mechanism of tyre traction in snow, the Rolling Resistance Moment (RRM) created by the tyre deformation geometry due to tyre sinking depth is important. This RRM causes Rolling Resistance Force (RRF) which opposes the vehicle motion, in addition to motion resistance in acceleration.
- Lagrangian Finite Element Method (FEM), Coupled Eulerian Lagrangian (CEL) and Smoothed Particle Hydrodynamics (SPH) numerical methods have been compared for the suitability to model tyre-snow interaction. SPH with cubic kernel function and with the uniform particle density of 10 mm between particles coupled with FEM for the structural analysis has been identified as a suitable numerical method to model tyre-snow interaction and used in all tyre-snow interaction analyses.
- The water removal process of sipes at contact patch and the difference in friction coefficient of rubber blocks with and without sipes have been shown using coupled FEM-SPH method. The block patterned tyre with sipes has been represented using a block patterned tread tyre with an equivalent friction coefficient which accounts the water layer created by the molten snow at contact patch due to frictional heat energy.
- A procedure to obtain longitudinal slip-force characteristics has been implemented using coupled FEM-SPH method and concluded that the longitudinal slip-force curve is not suitable for uncompacted snow terrain.
- To compare tyre performance and to identify the mechanism of tyre traction, torque-force characteristics have been used. From this study, the tyre sinking

depth of an uncompacted snow terrain is identified as an important factor that affects the tyre performance. The traction due to tread deformation, force due to compressed snow in tread grooves, motion resistance due to snow ahead of rolling tyre and the drawbar pull on tyre have been measured for smooth cap, block patterned tread and block patterned tread with sipes tyres for soft and hard snow with two different loads.

7.2 SCOPE OF FUTURE WORK

One of the major advantage of coupled FEM-SPH method is the capability of modeling large deformation problems without element distortion, contact penetration and convergence issues. Some of the possible options to extend this work in future are as follows,

- The lateral slip-force characteristics can be obtained using coupled FEM-SPH method.
- Tread optimization for maximum traction based on different tread depth, tread angle, tread pattern, edge effect and sipe stiffness can be made.
- An elastic-viscoplastic material model can be implemented instead of an elasto-plastic model for snow in numerical tyre-snow interaction analysis.
- The effects of snow temperature and frictional heat on change in material properties and frictional characteristics of tread can be experimented, modeled and used.

SPH elements are the Material Point Elements (MPE). Hence to assign mass for each MPE, ABAQUS constructs an imaginary volume around each MPE. To create these imaginary volumes, ABAQUS needs half of the distance between two nodes. This has to be given under *SOLID SECTION command as shown in Figure A.3. The corresponding kernel function can be given to SPH elements by *SECTION CONTROLS command as seen in Figure A.3.

```
*SOLID SECTION, ELSET=SNOW_ELEM, MATERIAL=SNOW, CONTROLS=SPH_CONTROL
0.005 ——— Half of the distance between nodes
*SECTION CONTROLS, NAME=SPH_CONTROL, KERNEL=CUBIC
|
| Corresponding Kernel function
```

Figure A.3: Input parameters for SPH elements

From density and imaginary volume values, the lumped mass can be assigned to each SPH elements. Thus SPH domain should be meshed more uniform (the distance between nodes should be identical) to assign uniform mass for all SPH elements.

In this study, all SPH snow models are rectangular slabs. Hence the mesh is uniform and masses are distributed evenly.

REFERENCE

1. **Brown, R.** (1989). Perspective on mechanical properties of snow. *Proc. 1st Int. Conf. Snow Eng*, (pp. 502-503).
2. **Browne, A.** (1974). Tire traction on snow-covered pavements. *The Physics of Tire Traction*, (pp. 99-139). Springer US.
3. **Bui, H. H., Fukagawa, R., Sako, K., & Ohno, S.** (2008). Lagrangian meshfree particles method (SPH) for large deformation and failure flows of geomaterial using elastic-plastic soil constitutive model. *International Journal for Numerical and Analytical Methods in Geomechanics*, 32(12), 1537–1570.
4. **Choi, J. H., Cho, J. R., Woo J. S., & Kim, K. W.** (2012). Numerical investigation of snow traction characteristics of 3-D patterned tire. *Journal of Terramechanics*, 49(2), 81–93.
5. **Colbeck, S. C.** (1982). An overview of seasonal snow metamorphism. *Reviews of Geophysics*, 20(1), 45–61.
6. **Continental Truck Tyre Report** (2016). *European regulations for winter equipment on trucks and buses European regulations for winter equipment on trucks and buses*. Hanover, Germany.
7. **Cresseri, S., & Jommi, C.** (2005). Snow as an elastic viscoplastic bonded continuum: a modelling approach. *Italian Geotechnical Journal*, 4, 43-58.
8. **Dhillon, R. S.** (2013). *Development of Truck Tyre-Terrain Finite Element Analysis Models*. Ph.D. Dissertation, University of Ontario Institute of Technology, Canada.
9. **Dunlop, J. B.** (1890). *U.S. Patent No. 441,649*. Washington, DC: U.S. Patent and Trademark Office.
10. **Ella, S., Formagne, P. Y., Koutsos, V., & Blackford, J. R.** (2013). Investigation of rubber friction on snow for tyres. *Tribology International*, 59, 292–301.
11. **Fernández, J. G.** (2012). *A Vehicle Dynamics Model for Driving Simulators*. Master's Thesis, Chalmers University of Technology, Goteborg, Sweden.
12. **Fierz, C., Armstrong, R. L., Durand, Y., Etchevers, P., Greene, E., McClung, D. M., ... Sokratov, S. A.** (2009). *The international classification for seasonal snow on the ground* (Vol 25), Paris: UNESCO/IHP.
13. **Fukuoka, N.** (1994). Advanced technology of the studless snow tire. *JSAE Review*, 15(1), 59-66.
14. **Fukuzaki, N., Yanaka, T., & Urushiyama, Y.** (1986). Effects of studded tires on

- roadside airborne dust pollution in Niigata, Japan. *Atmospheric Environment* (1967), 20(2), 377-386.
15. **Giessler, M., Gauterin, F., Wiese, K., & Wies, B.** (2010). Influence of Friction Heat on Tire Traction on Ice and Snow. *Tire Science and Technology*, 38(1), 4–23.
 16. **Gray, J. P., Monaghan, J. J., & Swift, R. P.** (2001). SPH elastic dynamics. *Computer Methods in Applied Mechanics and Engineering*, 190(49–50), 6641–6662.
 17. **Haehnel, R. B., & Shoop, S. A.** (2004). A macroscale model for low density snow subjected to rapid loading. *Cold Regions Science and Technology*, 40(3), 193–211.
 18. **Katakawa, K., Shimomura, C., Ishikawa, H., & Hatae, S.** (1992). Characteristics of snow pressure acting on avalanche-preventive fences. *In Second International Conference on Snow Engineering*, (pp. 323-331).
 19. **Lang, T., & Sommerfeld, R.** (1977). The modeling and measurement of the deformation of a sloping snow-pack. *Journal of Glaciology*, 19(81), 153-163.
 20. **Lee, J. H.** (2009). A new indentation model for snow. *Journal of Terramechanics*, 46(1), 1–13.
 21. **Lee, J. H.** (2011). Finite element modeling of interfacial forces and contact stresses of pneumatic tire on fresh snow for combined longitudinal and lateral slips. *Journal of Terramechanics*, 48(3), 171–197.
 22. **Lescoc, R.** (2010). *Improvement of Soil Modeling in a Tire-Soil Interaction Using Finite Element Analysis and Smooth Particle Hydrodynamics*, MS Thesis, The Pennsylvania State University, United States.
 23. **Liu, M. B., & Liu, G. R.** (2010). Smoothed particle hydrodynamics (SPH): an overview and recent developments. *Archives of computational methods in engineering*, 17(1), 25-76.
 24. **Meschke, G., Payer, H. J., & Mang, H. A.** (1997). 3D Simulations of Automobile Tires: Material Modeling, Mesh Generation, and Solution Strategies. *Tire Science and Technology*, 25(3), 154–176.
 25. **Monaghan, J.** (2000). SPH without a Tensile Instability. *Journal of Computational Physics*, 159(2), 290–311.
 26. **Nakajima, Y.** (2003). Analytical model of longitudinal tire traction in snow. *Journal of Terramechanics*, 40(1), 63–82.
 27. **Narasimha Rao, K.V.** (2005), *Design of Pneumatic Tyres with Finite Element*

- Analysis*, Ph.D. Dissertation, Indian Institute of Technology Madras, India.
28. **Nokian Winter Tyres Brochure** (2016). https://dc602r66yb2n9.cloudfront.net/pub/web/attachments/others/brochures/Nokian_Winter_Brochure_EN.pdf.
 29. **Pacejka, H. B.** (2006). *Tyre and vehicle dynamics*. Elsevier Butterworth-Heinemann, 2012, Third edition.
 30. **Reveles, J. R.** (2007). *Development of a Total Lagrangian SPH Code for the Simulation of Solids Under Dynamic Loading*. Ph.D Dissertation, Cranfield University, United Kingdom.
 31. **Ripka, S., Lind, H., Wangenheim, M., Wallaschek, J., Wiese, K., & Wies, B.** (2012). Investigation of Friction Mechanisms of Siped Tire Tread Blocks on Snowy and Icy Surfaces. *Tire Science and Technology*, 40(1), 1–24.
 32. **Seta, E., Kamegawa, T., & Nakajima, Y.** (2003). Prediction of Snow/Tire Interaction Using Explicit FEM and FVM. *Tire Science and Technology*, 31(3), 173–188.
 33. **Shapiro, L. H., Johnson, J. B., Sturm, M., & Blaisdell, G. L.** (1997). *Snow mechanics: review of the state of knowledge and applications* (No. CRREL-97-3), Cold Regions Research and Engineering Lab, Hanover, Germany.
 34. **Shoop, S. A.** (2001). *Finite Element Modeling of Tire – Terrain Interaction*. (No. ERDC/CRREL-TR-01-16), Cold Regions Research and Engineering Laboratory, Hanover, Germany.
 35. **SIMULIA Inc.** (2014). ABAQUS Version 6.14 documentation. Dassault Systemes, Simulia Corp., Providence, RI, USA, 2014.
 36. **Smith, F.** (1972). Elastic stresses in layered snow packs. *Journal of Glaciology*, 11(63), 407–414.
 37. **Smith, F., & Curtis, J.** (1975). Stress analysis and failure prediction in avalanche snowpacks. *IAHS Publication*. 114, 332-340.
 38. **Thomson, R.** (1847). *U.S. Patent No. 5,104*. Washington, DC: U.S. Patent and Trademark Office.
 39. **Voitkovsky, K., Bozhinsky, A., Golubev, V., Laptev, M., Zhigulsky, A., & Slesarenko, Y. Y.** (1975). Creep-induced changes in structure and density of snow. *IAHS Publication*, 114, 171–179.

LIST OF PUBLICATIONS

1. **Arunnelson X and R. Krishnakumar**, *Longitudinal Force Characteristics of Snow Tires using Coupled FEM-SPH Method*, 36th Annual Meeting and Conference on Tire Science and Technology, Akron, Ohio, USA, 12th-13th September 2017. (Accepted, email dt: 5/6/2017).

CURRICULUM VITAE

NAME : Arunnelson X

DATE OF BIRTH : 11th March, 1993

EDUCATIONAL QUALIFICATION

Master of Science (by Research)

Institution : Indian Institute of Technology Madras

Specialization : Engineering Design

Bachelor of Engineering (2014)

Institution : S.A. Engineering College

Specialization : Mechanical Engineering

GENERAL TEST COMMITTEE

CHAIR PERSON	:	Prof. Srikanth Vedantam Dept. of Engineering Design
GUIDE	:	Prof. R. Krishna Kumar Dept. of Engineering Design
MEMBERS	:	Prof. Raju Sethuraman Dept. of Mechanical Engineering Dr. Sankara J Subramaniam Associate Professor Dept. of Engineering Design